A critical perspective and analysis of two-step thermochemical fuel production cycles

Alon Lidor[a,*], Brendan Bulfin[b]

[a]*National Renewable Energy Laboratory, 15013 Denver West Parkway, 80401, Golden, CO, USA*
[b]*School of Chemistry & Environmental Research Institute, University College Cork, Cork, Ireland*

Abstract

Two-step thermochemical fuel production cycles powered using concentrating solar systems offer a route to convert solar energy to chemical fuels. In this work, we offer a critical assessment of the state of the art, a detailed technical analysis of this technology in terms of theoretical limitations and potential performance, and potential paths forward in the development of these processes. The state of the art for demonstrated reactor systems is analyzed using key performance indicators including energy efficiency, feedstock conversion extent, power output, and volumetric power density. The technical analysis first looks into the theoretical limitations on the cycles' process conditions and the role of the redox material. This is followed by a detailed thermodynamic analysis of the state-of-the-art CeO_2-based cycle, based on fixed bed mixed flow reactors, which closely represent the reactor designs used in demonstrations. Finally, a scale-up analysis is performed for the CeO_2-based cycle. The results from the theoretical analysis agree well with trends seen in experimental demonstrations of the concept. From the analysis, the low power density of the CeO_2-based cycle is highlighted as a critical design limitation that will seriously restrict further scale-up of this technology. We share perspective on this and other issues, and offer some outlook for future development.

Keywords: Solar fuels, Solar thermochemical fuel production, System analysis, Renewable fuels

Nomenclature

---

*Corresponding author. Email: alon.lidor@nrel.gov. The concept for this work was conceived while the authors were affiliated with ETH Zürich, but the work was performed while working at the National Renewable Energy Laboratory and University College Cork.

Roman symbols

c_p Specific heat capacity (mass based), $\mathrm{J\,kg^{-1}\,K^{-1}}$

ΔG Gibbs free energy, $\mathrm{J\,mol^{-1}}$

ΔH Enthalpy, J

ΔS Entropy, $\mathrm{J\,K^{-1}}$

E Energy, J

h Specific enthalpy (mass based), $\mathrm{J\,kg^{-1}}$

$\bar{h}$ Specific enthalpy (mole based), $\mathrm{J\,mol^{-1}}$

HHV   Higher heating value, $\mathrm{J\,mol^{-1}}$

LHV   Lower heating value, $\mathrm{J\,mol^{-1}}$

m Mass, kg

$\dot{m}$ Mass flow rate, $\mathrm{kg\,s^{-1}}$

n Amount, mole

p Pressure, bar

P_{out} Power output, W

Q Heat, J

$\dot{Q}$ Heat flow, W

R Universal gas constant, $\mathrm{J\,mol^{-1}\,K^{-1}}$

T Temperature, K

t Time, sec

V Volume, $\mathrm{m^3}$

W	Work, J
X	Conversion extent

Greek symbols

δ	Nonstoichiometry extent
$\varepsilon_{\mathrm{HR}}$	Heat recovery effectiveness
η	Efficiency
ρ	Density, $\mathrm{kg\,m^{-3}}$

Subscripts

aux	Auxiliary
chem	Chemical
conv	Convection
cw	Cooling water
e	Exit
i	Inlet
ox	Oxidation
rad	Radiation
red	Reduction
rerad	Reradiation
sens	Sensible heat
sg	Sweep gas

Abbreviations

CPV   Concentrated solar photovoltaic cell

CSP   Concentrating solar power

CV   Control volume

DNI   Direct normal irradiation

HTF   Heat transfer fluid

PEM Proton exchange membrane

RPC Reticulated porous ceramic

TES   Thermal energy storage

1. Introduction

Two-step thermochemical fuel production cycles powered by concentrating solar technologies have been suggested as a promising pathway to produce renewable fuels [1, 2, 3, 4, 5]. The general concept is to use optical concentrating systems to increase the natural solar irradiance of approximately $1 \, \mathrm{kW \, m^{-2}}$ by several orders of magnitude [6], resulting in a high flux that can exceed $1 \, \mathrm{MW \, m^{-2}}$, and offer a source of renewable high-temperature process heat to drive chemical reactions [7]. In 1977, Fletcher and Moen proposed that concentrating solar energy could be used to drive the thermolysis of water at high temperatures for the production of hydrogen [8], via the reaction,

$$\mathrm{H_2O} \longrightarrow \mathrm{H_2} + \frac{1}{2}\,\mathrm{O_2}. \tag{1}$$

The direct thermolysis presents a significant challenge due to the need to separate a mixture of $\mathrm{H_2}$ and $\mathrm{O_2}$ gases at high temperatures.

The two-step thermochemical redox cycle route inherently separates the $\mathrm{H_2}$ and $\mathrm{O_2}$ products. In this process a metal oxide is first reduced, releasing oxygen in a high-temperature endothermic reaction.

$$\mathrm{MO}_x \longrightarrow \mathrm{MO}_{x-1} + \frac{1}{2}\,\mathrm{O_2} \tag{2}$$

Provided the reduced metal oxide has a strong enough oxygen affinity, it can then be used to split both H_2O and/or CO_2 via an endothermic oxidation of the metal oxide:

$$MO_{x-1} + H_2O \longrightarrow MO_x + H_2 \tag{3}$$

$$MO_{x-1} + CO_2 \longrightarrow MO_x + CO \tag{4}$$
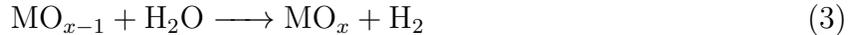
The metal oxide can then be recycled, with the net process converting high-temperature process heat into chemical energy in the form of hydrogen or syngas (see Figure 1). Furthermore, the two-step nature allows for the possibility of a temperature swing, making a heat engine that can perform additional chemical work during the lower-temperature oxidation step, and lowering the overall temperature requirement for the thermal splitting process [9].

In recent years, a number of high-profile demonstrations of this concept have been performed with up to 150 kW of input concentrating solar thermal power [10, 11, 12]. Syngas produced via this process can be further refined to liquid fuels, and with growing concern about our reliance on fossil fuels and their corresponding greenhouse gas emissions, it has been touted as a promising pathway to renewable fuels.
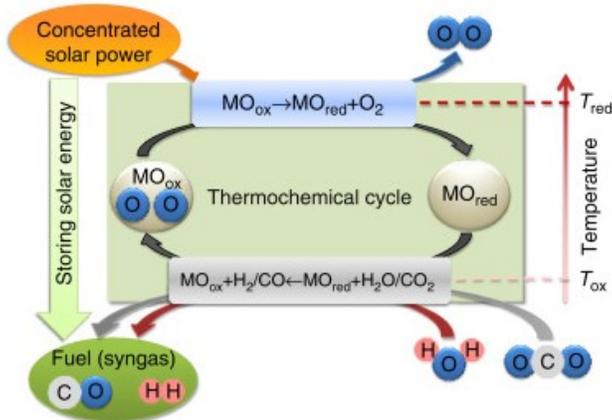
Figure 1: A general scheme of the two-step thermochemical redox cycle for syngas production (reprinted from Agrafiotis *et al.* [13] with permission from Elsevier).

In this work we offer a critical assessment of the state of the art for this energy conversion technology, a detailed technical analysis of its theoretical and practical limitations, and finally discuss the challenges in its further development. The analysis is valid for both solar thermochemical hydrogen production (STCH) and the production of so-called drop-in

fuels. The state of the art is presented in terms of the demonstrated performance of this process concept using performance indicators, including efficiency, feedstock conversion, power output, and power density. We then look at the fundamental thermodynamic limitations of these two-step cycles and their implications on process design. A more detailed technical analysis of the process based on the state-of-the-art material CeO_2 is also presented, with the inclusion of irreversible losses and practical limitations inherent in real systems. We then perform a power density and scale-up analysis based off the theoretical cycle performance. Finally, we discuss potential pathways for improving the performance of this technology and offer insight for future developments in both materials and process design.

1.1. Performance indicators

To benchmark demonstrations of two-step thermochemical fuel production reactors, we apply the following key performance indicators: energy conversion efficiency, power output, power density, and feedstock conversion [14].

Reactor Efficiency: The reactor energy conversion efficiency is given by,

$$\eta = \frac{n_{\text{fuel}}\text{HHV}_{\text{fuel}}}{Q_{\text{solar}} + Q_{\text{aux}}}, \tag{5}$$

where the numerator is the heating value of the fuel produced, Q_{solar} is the total solar power supplied to the reactor, and $Q_{\text{aux}} = \frac{W_{\text{aux}}}{0.4}$ is the equivalent heat required to power auxiliary processes (W_{aux}) including sweep gas generation and vacuum pumping during reduction. Note that since we have a cyclic process, each term needs to be integrated over at least one complete cycle. It is also important to note that Q_{solar} is the solar energy supplied to the reactor. While this efficiency is often referred to as solar-to-fuel efficiency in the literature, it is important to note that it does not include collection losses or spillage (concentrated flux that falls outside the reactor aperture), which can exceed the solar fluxes supplied to the reactor in many demonstrations. Furthermore, Q_{aux} is omitted in some reported values, or incomplete, neglecting for example the heat required for steam generation.

Power Output: In the literature, the scale of these systems is usually represented by stating their solar power input. However, for energy conversion devices in general it is more common to characterize the scale of systems by their power output. It is important to note that the power output for these systems is not simply the efficiency times the power input, since many

demonstrations use a single reactor with a cyclic batch process, where solar power is only input to the system during the endothermic reduction step. The power output is defined as,

$$P_{\text{out}} = \frac{n_{\text{fuel}}\text{HHV}_{\text{fuel}}}{t_{\text{cycle}}}, \tag{6}$$

where the numerator is the heating value of the fuel produced per cycle, and the denominator is the cycle time. In some cases continuous power input is achieved using multiple reactors, in which case the power output is directly related to the efficiency, $P_{\text{out}} = \eta(P_{\text{solar}} + P_{\text{aux}})$.

Power Density: Another important parameter for benchmarking the performance of these systems is their power density, both specific and volumetric. For comparison to other technologies, our system should include the reactor itself and auxiliary devices such as vacuum pumps which are directly supporting the operation of the reactor system. To simplify our initial comparison we use volumetric power density as a performance indicator, and we only count the active reactor volume (neglecting insulation, housing and auxiliary devices). This simplification is also partially due to the availability of this volume data. The volumetric power density is then the output fuel heating value per unit time and unit volume,

$$\text{Power density} = \frac{P_{\text{out}}}{V_{\text{Reactor}}}. \tag{7}$$

This power density can be considered as an upper-bound since it omits insulation and auxiliaries. The performance indicator is very important when considering reactor scale-up, as it allows the reactor volume necessary for a greater production rate to be estimated. Reactor volume is a crucial design constraint, which has implications for practical feasibility and cost.

This performance indicator has not received due attention to date. To highlight its importance, consider the power density from the most recent demonstration of Zoller *et al.* of 6.9 kW m^{-3} given in Table 1 [12]. With this power density a power output of 1 MW would require a reactor volume of 145 m^3 (not including insulation, peripheries). This is a very large size for what is a modest power output, and raises questions about the practical feasibility of further scale-up for this particular reactor concept. For comparison to other competing energy conversion technologies, Bosch offers a proton exchange membrane (PEM) electrolysis stack, which has a power output density of 785 kW m^{-3} (see supplementary information for

7

details). This is two orders of magnitude greater than Zoller's demonstration, which did not include the insulation, reactor housing or auxillary equipment such as vacuum pumps, in the system volume.

It is tempting to assume that increasing the efficiency will also directly increase the power density, but this is not necessarily the case. Many strategies for improving the efficiency consist of reducing the solar energy demand per cycle Q_{solar} using heat recovery. However, the power density only depends on the cycle time, fuel production rate, and reactor volume, and will not improve if only Q_{solar} decreases. In fact, additional auxiliary equipment such as gas-gas heat exchangers or packed beds for solid phase heat storage and recovery, would further reduce the power density of the whole device [15]. Instead, achieving greater power density will require reactors with more densely filled redox material, materials with larger oxygen storage capacities, and shorter cycle times.

Feedstock Conversion: The feedstock conversion extent is used to benchmark how effective the chemical conversion process is,

$$X_{\text{H}_2\text{O}} = 1 - \frac{n_{\text{H}_2\text{O, out}}}{n_{\text{H}_2\text{O, in}}}, \tag{8}$$

which is the fraction of feedstock fed to the reactor which undergoes a chemical reaction. Assuming we have ideal selectivity, the conversion extent is equivalent to the yield [14]. The importance of this performance indicator for chemical reactors is clearly evident in classical chemical engineering texts [16], where reactor performance equations relate the volume and input flow rate to the conversion extent. Consider for example a reactor with a relatively low conversion of 10%, requiring a feedstock flow rate which is 10 times higher than the desired production rate. In this case, excessive flow rates and feedstock recycling will have serious implications for the energy demand, practical feasibility, and ultimately the cost of the process. For the cyclic process considered here, the feedstock conversion needs to be integrated over the whole oxidation time.

Cycle Stability: One final measure of performance, which is not quantified numerically here, is the cycle stability, *i.e.* how do the other performance indicators change over multiple cycles, and how frequently do the reactors suffer from component failures. As these are not always reported they are simply discussed in cases where some conclusions can be made.

Ideally the reactors should should exhibit good performance in all performance indicators over a long time period.

1.2. State of the art

It is important to say that we are not providing a comprehensive review of experimental test campaigns on two-step solar thermochemical reactors here. In many cases, the data collected and reported is insufficient to determine the relevant performance indicators. Instead, we only include demonstrations that have reported the data required to calculate some of the performance indicators.

Many early efforts in this field focused on oxides that undergo a complete phase change upon reduction, such as ZnO [17] and Fe_3O_4 [18]. As seen in Table 1 both Gokon *et al.* and Driver *et al.* tested reactors based on iron oxides. These demonstrations resulted in low efficiency ($< 1\%$) and poor feedstock conversions. The low feedstock conversion is due to the small temperature swing used and the relatively low oxygen affinity of the Fe based oxides [19, 18]. This in turn affects the efficiency due to the need for excess steam generation. In fact, there have not been any experimental reactor demonstrations to date, which indicates that iron-based oxides have a promising outlook in any of the performance indicators applied here.

ZnO has arguably the best thermodynamic outlook of the cycles tested, due the large stoichiometric oxygen storage in this cycle combined with a relatively large entropy change upon decomposition to gaseous species, and its strong oxygen bond. However, demonstrations of this cycle have not yet yielded efficiencies above 1% [20]. The major issue with this process is that zinc oxide decomposes into Zn and O_2 gases, which readily recombine when cooled. It is very difficult to suppress this reverse reaction, with most of the reduced zinc simply re-oxidizing in the demonstrations shown in Table 1.

With the challenges faced in the above cycles, more recent demonstrations have tended to utilize the non-stoichiometric redox material CeO_2. There are several reasons why CeO_2 has made such a popular choice for demonstrations. Its strong oxygen bond allows the reduced oxide to react readily with H_2O and CO_2, with the potential for high feedstock conversion. It also undergoes partial reduction, which increases with increasing temperature [19, 22, 30], allowing flexibility in the process conditions. Finally, it exhibits very good chemical stability

Table 1: Reactor type, process conditions, and performance indicators for several demonstrations of two-step thermochemical fuel production cycles [10, 11, 12, 21, 22, 23, 24, 25, 26, 20, 27, 28]. A recent demonstration of a competing solar fuel production technology is also included as a benchmark [29].

Source	Reactor Type	Redox Material	Process conditions				Performance Indicators			
			C [-]	P_{solar} [kW]	T_{red} [K]	T_{ox} [K]	η (%) [-]	P_{out} [kW]	P_{out}/V [kW m^{-3}]	X_{H2O} (X_{CO2}) [-]
Gokon et al. 2008	DI cavity FB	$NiFe_2O_4$	2300	1.2	1673	1273	< 0.3 *	0.0008	28.3	-
Chueh etal. 2010	DI cavity M	CeO_2	1500	1.9	1773	~1273	0.8	0.0075	9.1	0.081 (0.067)
Diver et al. 2010	DI - RC	Fe_3O_4	-	-	1773	1573	-	-	-	(0.0005)
Miller et al. 2012	DI - RC	CeO_2	-	10.4	1893	1250-1350	0.66	0.05565	6.6	(0.0066)
Villasmil et al. 2014	DI cavity PF	ZnO	2500	8	1822	-	0.16	0.013	-	-
Hathaway et al. 2016	ID cavity PB	CeO_2	2400	4.4	1750	1750	0.72	0.069	50	(0.0075)
Koepf et al. 2016	DI cavity PF	ZnO	4600	100	2000	-	0.24	0.12	0.5	-
Marxer et al. 2017	DI cavity RPC	CeO_2	3260	4.1	> 1773	873-1273	5.25	0.079	45	(0.184)
Haeussler et al. 2020	DI cavity RPC	CeO_2	1474	1.5	1673	973-1073	< 1 *	0.001	4.3	(0.2)
Schäppi et al. 2021	DI cavity RPC	CeO_2	2700	5	> 1673	873-1273	1.9-3.8	0.03-0.08	4.8-12.8	0.03-0.05 (0.15-0.38)
Thanda et al. 2022	DI cavity RPC	CeO_2	549	155.2	1673	< 1273	< 0.45 *	0.35	1.1	0.011
Zoller et al. 2022	DI cavity RPC	CeO_2	2500	42	> 1773	873-1173	4.1	0.304	6.9	0.05 (0.1)
Holmes-Gentle et al. 2023	CPV + PEM	-	800	10.38	340	340	25	2.6	612	0.85

* Efficiency omits auxiliary work

Reactor acronyms, DI - directly irradiated redox material, ID - indirectly irradiated, FB - fluidized bed, PF - particle flow, PB - packed bed, M - monolith, RC - rotating cylinder

over many redox cycles [31]. On the downside it is difficult to reduce, with only small amounts of oxygen stored per cycle negatively impacting the practicality and efficiency.

Chueh *et al.* performed a breakthrough demonstration for the CeO_2 cycle [22], adopting a cavity design which was lined with a porous CeO_2 monolith. A high flux solar simulator supplied a concentrated flux of solar incident radiation into the cavity and directly onto the CeO_2 monolith. Reactor efficiencies fell short of 1% as can be seen in Table 1, but the reactor design proved to be robust and reliable, and was adopted and improved in several later demonstrations with improved performance.

Hathaway *et al.* also successfully utilized CeO_2 in a demonstration of isothermal fuel production [26]. In this case the redox material allows for what is essentially a separation enhanced thermolysis of CO_2. They used six packed bed reactors with integrated gas phase heat exchangers assembled in a solar cavity. The system was run continuously with three reactors operating in reduction mode while the other three underwent oxidation. The relative ease of continuous operation in this case is certainly a major draw over the temperature swing

cycles, but the feedstock conversion is thermodynamically limited to very small values with less than 1% conversion achieved. This in turn will also negatively impact the efficiency due to excessive heating and recycling of the feedstocks [32, 33]. Indeed, this system also failed to exceed 1% reactor efficiency. On the upside, this system exhibited the highest power output density of all the systems given in Table 1. The greater power density, despite the low efficiency, can be attributed to: 1) the use of indirectly heated packed bed reactors, with a greater packing density than the open volume directly irradiated cavity reactors, and 2) the isothermal operation allowing for short cycle times.
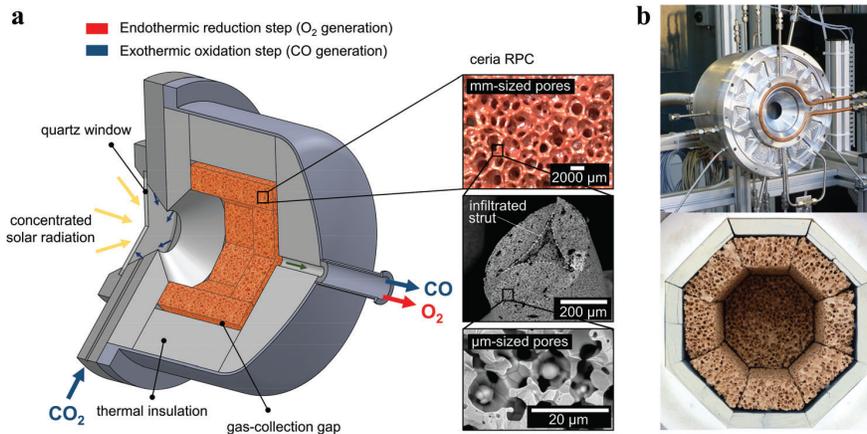
Figure 2: A schematic of the directly irradiated cavity reactor tested by Marxer *et al.* , copied from [34]. This type of reactor design has proven very popular for its relative simplicity with the same general design used in many other demonstrations [10, 11, 12, 22, 28].

The best all-around performance to date (in terms of efficiency, power density and feedstock conversion) was in the demonstration of Marxer *et al.* [27], which can be considered as an improved successor to the reactor tested by Chueh *et al.* [22]. Figure 2 shows a schematic of the reactor. Several design improvements were made over the original cavity reactor. Poor heat transfer into the CeO_2 was identified as a critical issue limiting the oxide utilization. A reticulated porous ceramic (RPC) structure was adopted instead, with large mm-scale pours allowing incident radiation to penetrate further into the structures and smaller μm-scale pours to allow for good mass transfer properties in the solid gas reactions. Another key design improvement from an efficiency perspective was the use of a vacuum pump and a small amount of sweep gas to achieve low oxygen partial pressures during reduction, as opposed to an inert sweep gas alone, as employed by Chueh *et al.* [22]. Finally, the Marxer reactor

used higher temperature reduction and a larger temperature swing, which has benefits for the oxidation reaction and its fuel yield. A point worth mentioning here is that while the RPC reduction temperatures reported by Marxer *et al.* is 1773 K, the thermocouples that measure this value are placed on the outer side of the RPC. The inner surface in the cavity is incident with radiation and a significant temperature gradient is expected across the RPC due to the still relatively poor thermal transport properties of such porous ceramic structures. Indeed, the relatively large extents of non-stoichiometry achieved during reduction do indicate significantly higher average temperatures in the RPC, even greater than 1873 K were achieved. The high incident flux combined with high reduction temperature are theoretically predicted to improve efficiency (see section 3 and [33, 32]). The net result was an efficiency of 5.25%, which represents a very significant increase over prior demonstrations. Furthermore, the power density and feedstock conversion are among the best demonstrated to date for this technology. Instantaneous feedstock conversions during oxidation peaked at values above 80%.

There are higher efficiencies reported in the literature for similar cavity RPC reactor designs tested by Abanades *et al.* [28, 35] with efficiencies values up to 9% quoted in the abstracts. However, these efficiencies were calculated as the peak power output divided by the power input, which is not a suitable efficiency definition for a cyclic process with varying power input and output. Here we recalculated the efficiency and other performance indicators for complete cycles in one of these studies [28]. The performance falls short of that reported by Marxer, which is expected due to the lower solar concentration and the lower reduction temperature achieved [8, 32].

Schäppi *et al.* demonstrated the whole solar-to-fuel process chain using the same reactor design as Marxer, with two reactors mounted on a solar dish system [10]. This allowed for continuous utilization of the incident solar power. Note that the goal of this demonstration was very broad in scope, demonstrating the production of renewable fuel using just solar power and the components needed for using air as a feedstock. Here we restrict our discussion to that of the reactor performance, which fell short of that of Marxer *et al.* . This is not surprising given that this demonstration used a real solar concentrating system as opposed to a solar simulator, having to cope with practical challenges such as higher reradiation losses

12

due to a larger aperture, and the variable DNI.

Thanda *et al.* tested a scaled-up system using a large high-flux solar simulator at the German Aerospace Center to deliver 150 kW of input solar power [11]. Again, this reactor utilized a directly irradiated cavity lined with supported CeO_2 RPC structures. This reactor was much larger than prior tests, with a total cavity plus RPC volume of around 300 liters, with previous volumes on the order of deciliters [27, 36]. They used a sweep gas instead of a vacuum pump, and the energy demand for generating this was not included in the reported efficiency given in Table 1. Generally speaking, the reactor performance was very poor, with low efficiency, fuel conversion, and power density, despite the larger scale. The low performance can be attributed to the low solar concentration used, which limited the temperature achievable during the reduction step and resulted in high re-radiation losses. There was also an unwanted reduction of the back of the RPC during oxidation by the produced H_2 due to a large non-stoichiometry gradient across the RPC [37]. This affects the feedstock conversion and quantity of fuel produced per cycle, which in turn decreases the efficiency.

Another larger-scale system was recently reported by Zoller *et al.* [12], which is a direct successor to the reactor of Marxer *et al.* , following the same design principles, but on a larger scale [38]. Again the scope of this demonstration was broader than just the reactor, with the production of syngas and the whole integrated liquid fuel process demonstrated. The successful execution of this demonstration has been touted as a major achievement in this field, due to its scale and complexity [39]. Having said that, despite its larger scale, the exemplary cycle reported for this system still falls short of its predecessor in terms of reactor performance indicators [27]. The authors do report a cycle with a higher efficiency of 5.6% ($\pm$ 1 %). The lack of a significant improvement in efficiency is somewhat surprising as one would expect a larger-scale system to suffer lower heat losses. This system did have a lower solar concentration, but achieved similar temperatures during reduction, again with the measured reduction temperatures at the outer side of the RPC. In this case the temperature gradient across the RPC was measured. This scaled demonstration indicates that the energy efficiency of these systems cannot be drastically improved simply by scaling them up, and new reactor and process design strategies are likely needed.

13

A significant drawback that can be taken from the demonstration of Zoller *et al.* [12], is that of a low power density. The scaled-up system of Zoller *et al.* exhibited a power output density which was a factor of 6 lower than that of Marxer *et al.* . Furthermore, despite a scale-up in power input by a factor of 10, the time-averaged power output is only increased by a factor of 4. This highlights the difficulty with scaling-up the open cavity reactor design. To have sufficient redox material in a larger cavity reactor system requires a large open volume, with a relatively thin outer shell of CeO_2 RPC. The reactor is therefore mostly empty space. The larger size and thermal mass also required longer cooling times between reduction and oxidation steps, meaning relatively less time with input solar power. The combined effect gives a much lower power density compared to the smaller reactor of Marxer *et al.* . The issue of low power density will need to be addressed if further scale-up is to be practically realizable. Moving away from open cavity directly irradiated reactors could help to address this, but would introduce its own challenges due to the very high temperatures required and the lack of commercial receivers operating in that range.

Recent work has aimed to address the issues of heat transfer into RPC structures in open cavity receivers, using instead 3D graded porous hierarchical structures [40, 41, 42, 43]. The main idea is to improve the radiative heat transfer, allowing for larger mass loading and more uniform heating in a directly irradiated CeO_2 structure, where the authors do show promising results. Having said that, the best performing structures still use large empty volumes to allow incident radiation to propagate into the structures. Batch reactors consisting of large, mostly empty cavities undergoing a large temperature swing cycle will likely offer poor performance in terms of power density.

It is worth noting that the trends in both efficiency and fuel conversion for the demonstrated systems follow quite well those predicted in theoretical thermodynamic analysis of solar thermochemical fuel production via this process [8, 32, 44], and are in good agreement with our analysis performed in section 3. Greater solar concentrations lead to lower radiative heat losses and allow higher temperatures to be achieved [8]. Furthermore, higher temperatures and a large temperature swing leads to greater oxygen storage per cycle, and a greater driving forces for the reduction and oxidation reaction, respectively, giving more fuel per cycle and better feedstock conversion and efficiency [32, 44]. The demonstration of isothermal

operation at 1773 K, resulted in poor feedstock conversion and low efficiency [32, 33].

Another point worth discussing is the stability of these reactor systems. While CeO_2 has been shown to have very good chemical stability over many redox cycles [27, 31], the structural stability of the RPC structures in a cavity subjected to high incident solar fluxes and extreme temperature swings has not been rigorously tested. Sufficient data is not available (over thousands of cycles and operation hours) to make definite conclusions in this regard, but existing results indicate that this could become an issue. After 46 cycles Zoller *et al.* reported the formation of fractures in the RPC structures (see Figure S6 in that work), which they attribute to in-homogeneous incident radiation leading to hot spots and high thermal stresses (see supporting information [12]). The overall structure did remain intact, but it is concerning for longer term cycle stability.

To put the state of the art for this field into context we also include a demonstration of concentrated solar energy conversion for hydrogen production using more conventional technologies [29]. The system tested by Holmes-Gentle *et al.* utilized a solar dish to supply 800 suns of concentrated solar flux to a combined heat and hydrogen production system. The hydrogen production unit is made up of a commercially available multi-junction concentrated solar photovoltaic cell (CPV), which was water cooled and heat integrated with a commercially available proton exchange membrane (PEM) electrolysis system for water splitting. The combined system offered an exemplary conversion of solar energy to hydrogen with an efficiency of 25% and a power output of 2.6kW. This efficiency is based off the energy flow chart of figure 6 in Holmes-Gentle *et al.* with the inclusion of auxiliary power demands within the system [29]. Furthermore, this system operates continuously with a much better power density and with lower solar concentration than the two-step thermochemical cycles, requiring less expensive optical systems. In short, this system far outperformed the demonstrations of two-step thermochemical systems in all performance indicators. Of course, while striking this comparison needs to be treated with some caution. One drawback here is that the PEM electrolysis system is not suitable for direct syngas production. This pathway would need to utilize a reverse-water-gas shift (RWGS) process to produce syngas [45].

1.3. State-of-the-art summary

The direct production of syngas followed by fuel production via gas-to-liquid technologies has been successfully demonstrated via the two-step solar thermochemical route [10, 12]. There has also been progress in improving the performance indicators between generations of reactors [22, 27]. Having said that, to provoke discussion on the future development we want to offer here a more critical assessment, to highlight emerging issues.

Attempts at scale-up have highlighted some issues with the directly irradiated cavity reactor design in terms of the scaling of the power output, power density, and efficiency [12]. The scale of the demonstrations to date seem far less flattering when characterized by their power outputs as shown in Table 1. The power output in the most recent demonstrations of Schäppi *et al.* , Thanda *et al.* and Zoller *et al.* , were 80 Watts, 350 Watts and 300 Watts respectively. From the demonstrations to date, this technology has not yet reached a performance sufficient to warrant further scale-up and industrial deployment is still a distant goal. It would be constructive to have a discussion on how (and even if) this technology can be improved sufficiently for industrial deployment.

There are techno-economic analysis studies that have reported a more optimistic outlook [46, 47, 48]. However, a key point in these studies is that they assume the reactors will operate with very high performance, far in excess of those demonstrated to date. For example Moretti *et al.* assume reactor efficiencies in the range of 30 to 55% [48], with 30% used for near-term deployment scenarios. It is not at all clear how and even if these efficiency values can be achieved in practice, especially in the short term. For example, one of the most rigorous and complete thermodynamic analyses of this concept performed by Li *et al.* [44] set upper bounds on the efficiency in the region of 30%. They modeled an idealized counter-flow moving particle system, which maximizes the potential feedstock conversion and ceria reduction potential, and assumed a very optimistic 90% solid-to-solid heat recovery and 95% gas phase heat recovery, which gave a maximum efficiency of 26% [44]. Counter-flow moving particle reactors have yet to be demonstrated, as do such effective heat recovery systems. Unfortunately, it is safe to say that the performance required for competitive industrial deployment is not likely in the near term.

Another hurdle facing this technology is that the solar concentrations used in demonstra-

tions are much higher than what is typically available in industrial concentrating solar power (CSP) systems [6, 49]. Furthermore, there has been a significant slowdown in the growth of deployed CSP systems in recent years [49, 50]. This slow-down is a bit concerning for technologies which aim to use similar concentrating solar systems as there basis.

2. Thermodynamic principles & materials selection

The concept of using multi-reaction thermochemical cycles as a pathway to converting heat to hydrogen was analyzed in detail by Funk and Reinstrum as early as 1966 [9]. Furthermore, the fundamental limitations of combining concentrated solar radiation with thermodynamic heat to chemical work cycles was formulated by Fletcher and Moen [8]. Building upon this work there are also many theoretical studies focused on two-step thermochemical solar fuel production using CeO_2-based oxides [32, 51, 52, 53], and perovskite oxides [54]. Another area that has received a lot of attention are the different reactor and process design concepts [55, 56, 57]. While these studies cover the many variations of this process concept and their complexities, it is easy to get lost in the details. Here we present the basic thermodynamic principles of a two-step heat to chemical work conversion process to highlight the fundamental limitations of the process and use these as guiding principles to discuss material and process development.

The primary thermodynamic limitations of this process are those of the water-splitting reaction (or carbon dioxide-splitting). The thermodynamic equilibrium of the water-splitting reaction, given in Equation 1, can be described in terms of the change in Gibbs free energy of the reaction,

$$\Delta G_{\mathrm{ws}} = \Delta G_{\mathrm{ws}}^{\circ}(T) + \frac{1}{2}RT\ln\left(\frac{p_{O_2}}{p^{\circ}}\right) + RT\ln\left(\frac{p_{H_2}}{p_{H_2O}}\right). \tag{9}$$

where $\Delta G_{\mathrm{ws}}^{\circ}(T)$ is the standard change in Gibbs free energy for the water-splitting reaction, the second two terms represent the equilibrium constant term $RT\ln(K)$. If $\Delta G_{\mathrm{ws}} = 0$ then the reaction is in equilibrium for the given T, p_{O_2}, p_{H_2}, and p_{H_2O}. Otherwise ΔG_{ws} represents the chemical work per mole that is required to achieve those conditions. The standard change in Gibbs free energy for this reaction decreases with increasing temperature, meaning that the water-splitting reaction becomes more favorable at higher temperatures.

If we perform the water-splitting reaction in a two-step metal oxide redox cycle we then have the reduction reaction give in Equation 2, with a change in Gibbs free energy given by,

$$\Delta G_{\text{red}} = \Delta G_{\text{red}}^{\circ}(T) + \frac{1}{2}RT \ln\left(\frac{p_{\text{O}_2}}{p^{\circ}}\right) \tag{10}$$

Where the standard change in Gibbs free energy for the reaction can be separated into enthalpy and entropy terms,

$$\Delta G_{\text{red}}^{\circ}(T) = \Delta H_{\text{red}}^{\circ} + T\Delta S_{\text{red}}^{\circ} \tag{11}$$

which are commonly reported as the relevant materials properties. $\Delta H_{\text{red}}^{\circ}$ is closely related to the binding energy of oxygen in the oxide, and it is the heat input required to liberate the oxygen. $\Delta H_{\text{red}}^{\circ}$ would be the y-intercept at $T = 0\,\text{K}$ of the $\Delta G_{\text{red}}^{\circ}(T)$ line in Figure 3 **a**, and $\Delta S_{\text{red}}^{\circ}$ is the slope. For illustration here we assume an idealized case where the standard changes in enthalpy and entropy do not depend on temperature. In the case of non-stoichiometric oxides like $CeO_{2-\delta}$, these properties have a dependence on δ.

To undergo a purely thermal driven reduction reaction releasing oxygen at standard pressure ($\Delta G_{\text{red}}^{\circ}(T) = 0$), the oxide must reach a high temperature,

$$T_H = \frac{\Delta H_{\text{red}}^{\circ}}{\Delta S_{\text{red}}^{\circ}} \tag{12}$$

If the oxide is then cooled to a lower temperature for re-oxidation T_{ox}, it can be used to do thermodynamic work. The maximum amount of work that can be done per mole of atomic oxygen is,

$$W_{\text{max}} = \left(1 - \frac{T_{\text{ox}}}{T_H}\right)\Delta H_{\text{red}}^{\circ} = \Delta G_{\text{red}}^{\circ}(T), \tag{13}$$

which is the Carnot efficiency for the cycle temperatures, times the heat input of the reduction reaction. This is also equal to the change in Gibbs free energy for the reversible reduction reaction. This maximum work is illustrated in Figure 3 **a**, for the state of the art material $CeO_{2-\delta}$ with $\delta = 0.05$ [58].

The temperature for a purely thermal reduction reaction is generally very high. In practice the oxygen partial pressure is reduced by several orders of magnitude using either vacuum pumps or sweep gas, providing an input of work and reducing the reduction temperature T_{red},

$$W_{\text{O, red}} = \frac{1}{2}RT_{\text{red}} \ln\left(\frac{p_{\text{O}_2,\text{red}}}{p^{\circ}}\right) \tag{14}$$

Note that this reduces the temperature required for reduction, but it does not change the maximum work that can be done during the re-oxidation $W_{\mathrm{max}} = \Delta G_{\mathrm{red}}^{\circ}(T)$. If the cycle is performed isothermally, all of the input work is performed by reducing the partial pressure and $W_{\mathrm{max-iso.}} = W_{\mathrm{O,red}}$ which is also labeled in Figure 3.

The pumped or swept oxygen is typically cooled to close to ambient temperature before pumping or separation, meaning that the actual work input can be much lower than $W_{\mathrm{O,red}}$. Assuming an idealized isothermal vacuum pump operating at ambient temperature, the input work is given by,

$$W_{\mathrm{pump-min}} = \frac{T_{\mathrm{amb}}}{T_{\mathrm{red}}} W_{\mathrm{O,red}}. \tag{15}$$

While the large temperature change applied to the oxygen before pumping offers what is theoretical a very low work input, in practice vacuum pumps (or sweep gas separation) are subject to a lot of irreversible loses and typically operate with low efficiencies, which decrease with decreasing pressure [59].

Finally, to close the cycle the metal oxide is re-oxidized in H_2O as seen in Equation 3. The equilibrium of this reaction is given by,

$$\Delta G_{\mathrm{ox}} = \Delta G_{\mathrm{ox}}^{\circ}(T) + RT \ln \left(\frac{p_{\mathrm{H_2}}}{p_{\mathrm{H_2O}}} \right). \tag{16}$$

Since the oxidation and reduction reaction sum to give water splitting we can use the additivity of the thermodynamic properties to get $\Delta G_{\mathrm{ox}}^{\circ}(T)$,

$$\Delta G_{\mathrm{ox}}^{\circ}(T) = \Delta G_{\mathrm{ws}}^{\circ}(T) - \Delta G_{\mathrm{red}}^{\circ}(T). \tag{17}$$

Note that this means that $\Delta G_{\mathrm{ox}}^{\circ}(T) = 0$ when $\Delta G_{\mathrm{ws}}^{\circ}(T) = \Delta G_{\mathrm{red}}^{\circ}(T)$, at which temperature the oxidation reaction equilibrium $\Delta G_{\mathrm{ox}} = 0$, will yield $p_{\mathrm{H_2}} = p_{\mathrm{H_2O}}$. This corresponds to a maximum feedstock conversion of 50%.

2.1. Temperature swing cycles

With the basic thermodynamic limitations of the process we can begin to design the two-step cycle. Note that we have a lot of free parameters to fix. From the materials perspective we have the enthalpy and entropy of reduction $\Delta H_{\mathrm{red}}^{\circ}$ and $\Delta S_{\mathrm{red}}^{\circ}$. For the process conditions we have the reduction temperature T_{red}, the oxidation temperature T_{ox}, the reduction pressure
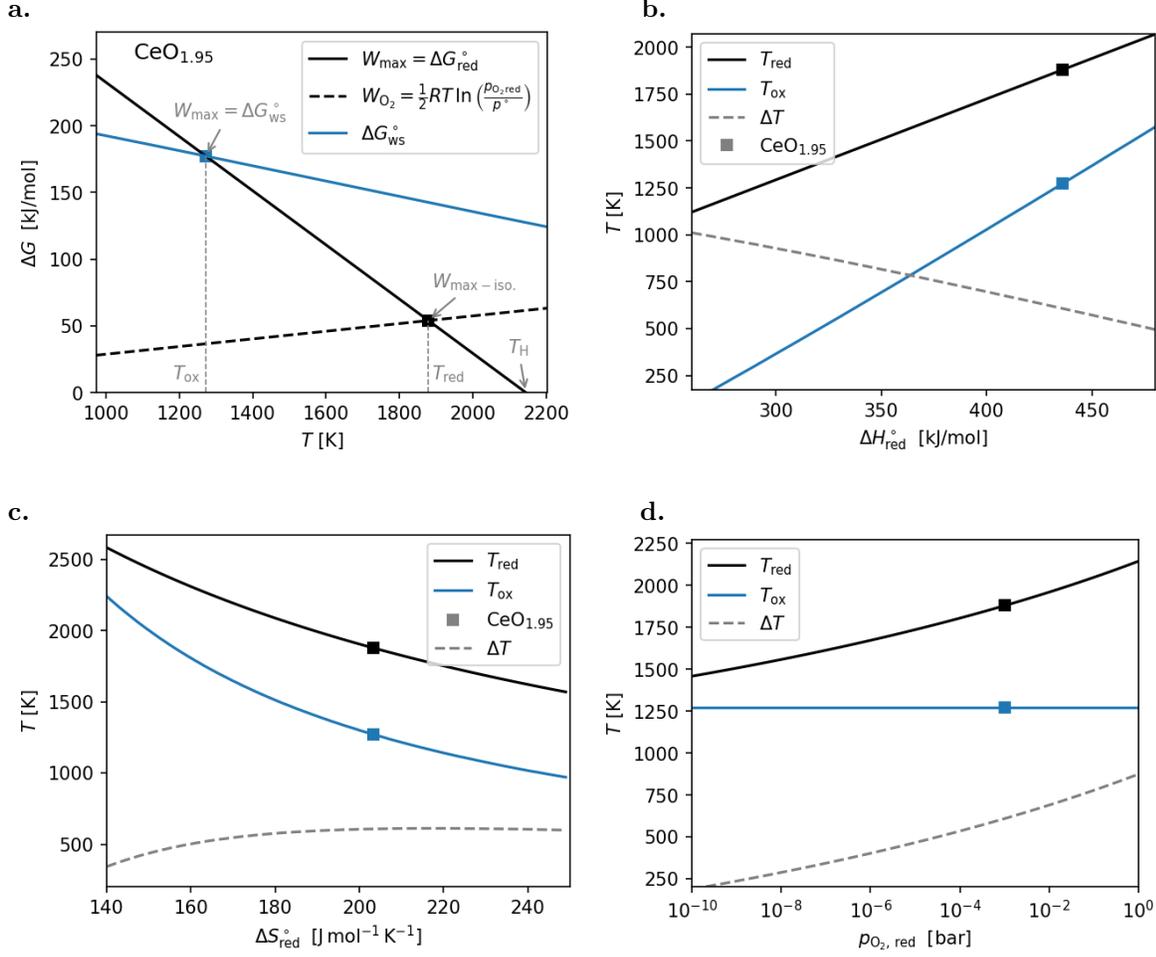
Figure 3: Temperature requirements for a two-step thermochemical cycle using the parameters of table Table 2 as the base case. **a.** An ellingham diagram showing the required work per mole to split water $\Delta G_{ws}^{\circ}(T)$ with a conversion extent of 50% and the work that can be done by the oxidation reaction of $CeO_{1.95}$, $\Delta G_{red}^{\circ}(T)$, with the resulting cycle temperatures labeled. **b.** The cycle temperatures plotted as a function of the enthalpy of reduction. **c.** The cycle temperatures plotted as a function of the entropy. **d.** The cycle temperatures plotted as a function of the reduction pressure $p_{O_2,red}$.

$p_{O_2,red}$, and the desired extent of water splitting in the oxidation reaction $\frac{p_{H_2}}{p_{H_2O}}$. We can begin to fix the parameters by setting goals based on our performance indicators.

The performance indicator we can most easily apply is the feedstock conversion extent, which is related to the ratio of steam to hydrogen by,

$$\frac{p_{H_2}}{p_{H_2O}} = \frac{X_{H_2O}}{1 - X_{H_2O}}. \tag{18}$$

Setting a reasonable goal for this parameter is crucial. Many studies, material screening

in particular, achieve or even set target values of $X_{H_2O} < 0.01$ [60, 61]. This would not result in a process which can be efficient or practically scaled-up. To use a very cliché example, the successful development of the Haber-Bosch process essentially boiled down to balancing the kinetic, thermodynamic, and practical limitations, while still achieving a meaningful conversion extent, typically exceeding 10% in industrial systems. Here we choose a desired conversion extent of 50%, which corresponds to $\frac{p_{H_2}}{p_{H_2O}} = 1$. A high conversion extent is very desirable given the very high temperatures that the feedstock must be heated to, where separation and recycling can introduce significant challenges if performed at these temperatures, or large energy penalties due to cooling and reheating.

Next we can also fix the reduction pressure. Based off previous demonstrations and the efficiency of vacuum pumps at lower pressure, we set a value here of $p_{O_2, red} = 10^{-3}$ bar. For the base case material properties we use those of $CeO_{2-\delta}$ with $\delta = 0.05$ [58]. The base case parameters are summarized in Table 2. Fixing the reduction pressure and materials properties also fixes the reduction temperature as illustrated in Figure 3 **a.**, while the conversion extent fixes the oxidation temperature.

Table 2: Base parameters for a two-step temperature swing fuel production cycles.

Material properties ($CeO_{1.95}$)		
ΔH°_{red}	436	$kJ\,mol^{-1}$
ΔS°_{red}	203	$J\,mol^{-1}\,K^{-1}$
Process conditions		
$p_{O_2, red}$	10^{-3}	bar
$\frac{p_{H_2}}{p_{H_2O}}$	1	-

Materials Selection

Having fixed the reduction partial pressure and the desired conversion extent, an obvious question is how do our choice of materials affect the required reduction and oxidation temperatures of the process. There are already quite a few studies in the literature that approach this problem using process models and the efficiency as a performance indicator, with different materials considered [62, 63, 64, 52]. There is also an excellent recent study

performed by Li *et al.* [51], which considers real as well as hypothetical materials, with a rigorous process model used to compare them with efficiency as a performance indicator, offering much needed guidance to the field of materials development and screening. Here we offer a more simplified view in terms of the required process temperatures, but it is enough to understand the basic fundamental limitations, and guide our discussion.

Figure 3 **b.** shows the effect of changing the reduction enthalpy, with the entropy and reduction pressure held constant. It can be seen that increasing the enthalpy of reduction increases the required reduction temperature, but due to the larger heat input per mole, a lower temperature swing is required to do the work of water splitting. Figure 3 **c.** shows the effect of changing the reduction entropy, where increasing the entropy of reduction decreases the required reduction temperature, with the required temperature swing remaining relatively unchanged.

Two of the major challenges facing this process are the high temperatures and the relatively large amounts of sensible heat required to cycle the oxide between the reduction and oxidation temperatures which affects the efficiency,

$$Q_{\text{sens.}-\text{solid}} = \frac{1}{\Delta\delta} \int_{T_{\text{ox}}}^{T_{\text{red}}} C_{p,\,\text{MO}_{\text{x}}} dT \tag{19}$$

Where $\Delta\delta$ is the change in stoichiometric oxygen in the cycle and $C_{p,\,\text{MO}_{\text{x}}}$ is the specific heat of the solid. With this in mind materials screening studies often state one or more goals, including;

- Increasing the oxygen storage capacity of the oxides for a given set of process conditions.

- Decreasing the high reduction temperatures T_{red}.

- Decreasing the temperature swing of the cycle ΔT.

The final two points actually present a *catch-22* for this technology. The enthalpy of reaction (the oxygen bond strength) can readily be tailored [64, 65], but we can see this route cannot satisfy both points, with a decreasing reduction temperature causing an increase in temperature swing. Furthermore, increasing the entropy, a difficult task, could also decrease the reduction temperature, but does not drastically affect the temperature swing. In the hypothetical material study of Li *et al.* [51], they conclude that both larger enthalpies and

entropies of reduction would be more beneficial for most materials considered. They hypothetical materials considered are variations of the known state-of-art non-stoichiometric oxides. They highlight that state-of-the-art CeO_2 and CeO_2-based oxides have the most promising performance. This study shows the need for careful consideration of the materials properties in tandem with a detailed process model.

The above bullet points are generally sighted as motivation in materials screening studies. However, a common trend has been to tackle these points while neglecting the importance of feedstock conversion, and benchmarking materials based only off the oxygen storage capacity [66, 67, 68]. Essentially, authors use a lower reduction temperature and a lower temperature swing, without paying due attention to the feedstock conversion limitations. This goes against the basic principles of chemical process design, and has led to limited progress in improving the outlook for this technology.

The thermodynamic work required to drive the water-splitting reaction decreases for a decreasing conversion extent according to the reaction equilibrium term $RT \ln \left(\frac{p_{H_2}}{p_{H2O}} \right)$. For the oxidation reaction performed at $1273\,\mathrm{K}$, the work required to achieve $p_{H_2} = x p_{H2O}$ for $x = 1$ and 0.01, is 177 and $128\,\mathrm{kJ\,mol^{-1}}$ respectively. It is therefore relatively trivial to satisfy the bullet points above if one sacrifices the feedstock conversion extent, as the cycle does less work.

Thermally driven water-splitting in two reaction steps requires a large amount of work per mole. This inevitably requires high temperatures, very effective oxygen removal, and/or large temperature swings according to the basic principles of heat-to-chemical work cycles. Higher temperatures should actually be favored according to theoretical studies [32, 44]. From a materials development perspective, durable performance at high temperatures is desired, with good oxygen storage, but not at the expense of feedstock conversion. There is currently little to suggest that game changing improvements can be made to the process simply via the discovery of new non-stoichiometric oxides [51]. Li *et al.* do show that modest improvements in efficiencies could be achieved with a material exhibiting the same reduction enthalpies as CeO_2, but larger reduction entropies than CeO_2. Yet, it is unclear if and how this could be achieved, given that CeO_2 already exhibits an exceptionally large entropy of reduction [69, 19]. One option would be to incorporate phase changes in the cycle [70], but this is

likely to affect the cycle stability. To summarize, a silver bullet is unlikely to emerge from these materials studies. The redox material cannot change the underlying thermodynamics limitations of thermal water-splitting.

Finally, it is worth noting that all of the bullet points above can be achieved by using a lower reduction pressure $p_{O_2,\text{red}}$ as illustrated in Figure 3 **d** for the temperature swing and reduction temperature. What this figure does not illustrate is that this will also allow greater extents of reduction δ, if the reduction temperature is not decreased accordingly. Therefore, a more obvious strategy for improvements would be to focus on this aspect of the cycle, as opposed to the redox materials themselves. This point has not been overlooked by the field, with several studies considering different oxygen pumping technologies [59, 71, 72, 73]. One issue that has perhaps been mostly overlooked (with the exception of [73]) is the very large flow velocities u, which would arise at such low pressures with $u \propto \frac{1}{p}$. This would require pumps and gas connections which can handle extremely large volumetric flow rates, and could lead to large pressure drops and/or limited oxygen removal rates, making the reduction step impractical. Even for the state-of-the-art systems operating at $p \approx 1mBar$, it is unclear what scale can be achieved with vacuum pumps currently available.

2.2. Isothermal cycles

Performing the two-reaction steps isothermally goes back to the original concept of Fletcher and Moen [8], which is a separation enhanced thermolysis. The role of the oxide is simply to absorb the oxygen in the oxidation step and allow it to be removed at low partial pressures in the reduction step [74].

Assuming that the reduction reaction reaches equilibrium, setting Equation 10 equal to zero gives,

$$\Delta G_{\text{red}}^{\circ}(T) = -\frac{1}{2}RT\ln\left(\frac{p_{O_2,\text{red}}}{p^{\circ}}\right) \tag{20}$$

Combining this with Equation 16 and Equation 17 gives an equilibrium condition for the oxidation,

$$\Delta G_{\text{ox}} = \Delta G_{\text{ws}}^{\circ}(T) + \frac{1}{2}RT\ln\left(\frac{p_{O_2,\text{red}}}{p^{\circ}}\right) + RT\ln\left(\frac{p_{H_2}}{p_{H_2O}}\right) = 0. \tag{21}$$

Which is the equilibrium condition for water-splitting, where the oxide terms cancel out in the summed reaction, making this condition material independent. This sets an equilibrium

24

upper-bound on the feedstock conversion given by,

$$\left(\frac{p_{H_2}}{p_{H_2O}}\right)_{eq} = \exp\left(\frac{-\Delta G^{\circ}_{ws}(T) + 0.5\ln(p_{O_2,red})}{RT}\right). \tag{22}$$

and,

$$X_{H_2O,max} = \left(\frac{p_{H_2}}{p_{H_2O}}\right)_{eq} \bigg/ \left(1 + \left(\frac{p_{H_2}}{p_{H_2O}}\right)_{eq}\right). \tag{23}$$

The maximum conversion is then only dependent on the temperature and oxygen partial pressure achieved during reduction. As illustrated in Figure 3 **a**, all of the work is done by the oxygen removal step. As described earlier this could be a very effective way of performing work on this system, due to the large difference between the reduction temperature and the operation temperature of the oxygen pumping step. However, achieving large feedstock conversions can be a significant challenge as can be seen in Figure 4, with high temperatures and low oxygen partial pressures necessary to achieve modest feedstock conversions. CO_2 thermolysis is more favorable than H_2O thermolysis at high temperatures, but a high conversion is even more crucial, due to the difficulty in separating the products. Note that these thermodynamic limitations are completely independent of the redox material used, where demonstrations of isothermal cycling to date do agree with these thermododynamic limits. For example taking the average values from Hathaway *et al.* [26] of $T = 1750\,K$ and $p_{O_2} = 0.00375\,bar$ (from oxygen outflow rates), Figure 4 gives a thermodynamic limit of $X_{CO_2} = 0.00742$ in good agreement with the average conversion reported (note the authors actually report a lower oxygen pressure and conversion of 0.0025, but we calculated 0.0075 based off their reported flow rates). This indicates that this reactor was operating very close to the thermodynamic limit, which one would expect for a plug-flow reactor at such high temperature.

Efforts on the isothermal cycles have focused largely on the development of new materials [75, 76, 77], and various methods of achieving low oxygen partial pressures [77], with only one notable experimental demonstration of an isothermal reactor system [26]. Materials development has typically focused on increasing the oxygen storage capacity of the materials, but this cannot improve the theoretical upper-bounds on feedstock conversion. Tran *et al.* recently demonstrated that oxygen storage capacity can also be increased by performing the oxidation at higher pressures [78], which increases the oxygen partial pressure in the
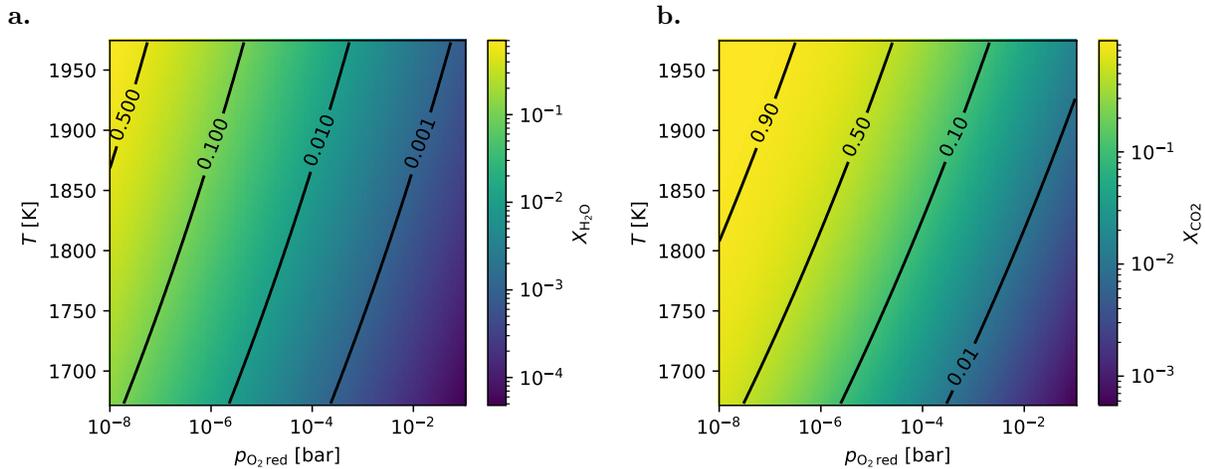
Figure 4: The feedstock conversion limits of an isothermal cycle plotted against the reduction partial pressure and the reduction temperature for **a.** H_2O thermolysis and **b.** CO_2 thermolysis.

feedstock, allowing for greater oxidation extents. However, the upper-bounds on feedstock conversion are still limited by the reduction pressure. As with the temperature swing cycles, Carrillo *et al.* identified the importance of achieving very low oxygen partial pressures and considered the energy demand of various oxygen removal methods [77].

One issue with most studies in the literature on isothermal cycles is that the temperatures considered are usually at or below $1773\,K$ [77, 78], where limitations in achieving low oxygen partial pressures will inevitably result in very poor feedstock conversion as can be seen in Figure 4. There has not been a convincing argument made for how this process could be practically scaled-up with such low feedstock conversions. While the isothermal route is attractive for its simplicity, and its potential for shorter cycle times and greater power densities, research efforts need to address the low conversion extent. The obvious route to improving feedstock conversion is to consider higher temperatures and improving the oxygen removal during reduction.

3. Real reactor limitations

Most existing theoretical analysis of solar thermochemical fuel production processes is focused on the thermodynamics of an ideal (or near ideal) system [8, 53, 79, 32]. This type of analysis is useful in calculating upper boundary efficiencies and to compare different redox materials. However, an unrealistically high performance is usually predicted by such

an analysis, with theoretical efficiencies much greater than what has been demonstrated experimentally. A more detailed system analysis has been performed mostly for flow reactors, namely co-current flow and counter-current flow configurations [80, 81, 55, 44]. The focus on counter-current systems in particular is attributed to their potential for better performance due to favorable chemical potential gradients and the possibility for heat recovery. However, these systems will require moving the redox material through reactors and heat ex-changers (e.g., in the form of particles), a feat that is yet to be experimentally demonstrated, and presents a significant technical challenge given the high temperatures.

Here we propose a more realistic analysis based on a fixed bed mixed-flow two-step cyclic batch reactor, assuming a uniform state across the volume. This idealized system is a good representation of the open cavity reactor designs that have proven most popular in experimental demonstrations. We also introduce the practical energy limitations that are often omitted from such an analysis: (a) heat losses to the ambient through the insulated shell of the reactor (in addition to reradiation losses which are usually considered); (b) transient heating/cooling losses to the inert reactor components due to the temperature cycling; (c) inert gas separation energy; (d) inert gas heating; (e) vacuum/sweep gas pumping energy; and (f) oxidizer required heating. Items (c), (d), and (e) are often omitted for sweep-gas operated reactors, while (f) is almost always omitted. Items (a) and (b) are rarely accounted for, but can significantly affect the performance.

3.1. Energy limitations

The energy balance on a control volume (CV) containing the entire solar reactor is:

$$\frac{dE_{\text{CV}}}{dt} = \dot{Q}_{\text{CV}} - \dot{W}_{\text{CV}} + \sum \dot{m}_{\text{i}} h_{\text{i}} - \sum \dot{m}_{\text{e}} h_{\text{e}} \tag{24}$$

The internal energy can be divided into three parts: (a) the sensible heat of the metal oxide E_{sens}; (b) the chemical reaction enthalpy (endothermic during reduction and exothermic during oxidation) E_{chem}; and (c) the sensible heat of the inert parts (insulation) E_{ins}.

The different heating terms are: (a) solar energy input (during reduction only) $\dot{Q}_{\text{solar}}$; (b) the reradiation losses $\dot{Q}_{\text{rerad}}$; (c) the convection losses from the shell $\dot{Q}_{\text{conv}}$; (d) the radiation

27

losses from the shell $\dot{Q}_{\mathrm{rad}}$; and (e) the heat lost to the cooling system (usually required to cool the quartz window or sealing parts) $\dot{Q}_{\mathrm{cw}}$.

The pumping work required to sustain a gas flow through the system (during reduction if using sweep gas, and at any other step with significant flow such as oxidation or heat recovery with a heat transfer fluid (HTF)), or the work required for reducing the pressure in a vacuum-operated system, are calculated separately as auxiliary energy input (Equation 5), since the work itself crosses the CV boundary of the pump/blower. Hence, there is no work performed within the reactor CV resulting in $\dot{W}_{\mathrm{CV}} = 0$.

The flow terms are as follows: (a) optional inert gas flow at a low flow rate next during all steps (protecting the window from particles, support the creation of desired flow patterns, etc.); (b) sweep gas flow during reduction (for sweep gas reactor); (c) HTF at high flow rate during heat recovery steps; (d) O_2 released from the redox material during reduction (outlet only); and (e) reactant and product flows during oxidation.

If we integrate over the time for a single operating step, solving for a general case (all terms), we get:

$$\Delta E_{\mathrm{sens}} + \Delta E_{\mathrm{chem}} + \Delta E_{\mathrm{ins}} = Q_{\mathrm{solar}} + Q_{\mathrm{rerad}} + Q_{\mathrm{conv}} + Q_{\mathrm{rad}} + Q_{\mathrm{cw}}+ \tag{25}$$
$$\int \dot{m}_{\mathrm{Ar}} \left(h_{\mathrm{Ar,i}} - h_{\mathrm{Ar,e}} \right) dt + \int \dot{m}_{\mathrm{sg}} \left(h_{\mathrm{sg,i}} - h_{\mathrm{sg,e}} \right) dt$$
$$\int \dot{m}_{\mathrm{HTF}} \left(h_{\mathrm{HTF,i}} - h_{\mathrm{HTF,e}} \right) dt-$$
$$\int \dot{m}_{O_2} h_{O_2} dt + \int \dot{m}_{\mathrm{ox,i}} h_{\mathrm{ox,i}} - \int \dot{m}_{\mathrm{ox,e}} h_{\mathrm{ox,e}} dt.$$

In this equation, Q_{solar} is positive (when applicable) while all the other heat terms (Q_{rerad}, Q_{conv}, Q_{rad}, Q_{cw}) are negative since they represent heat leaving the CV (Figure 5).

3.1.1. Energy change in the CV

The metal oxide energy change can be calculated if the temporal evolution of its temperature is given per:
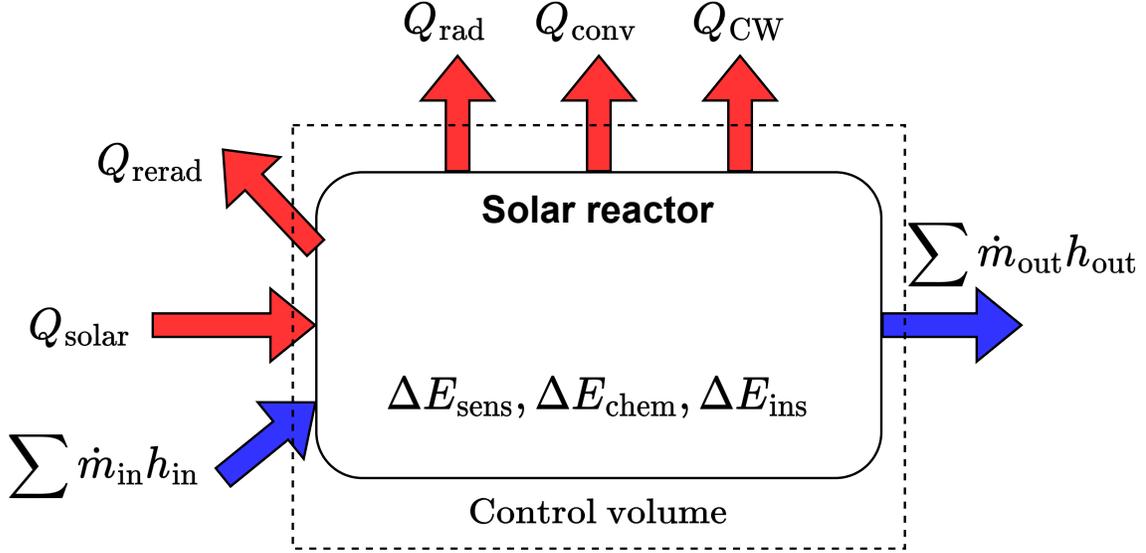
Figure 5: Control volume of the solar reactor including all the energy terms.

$$\Delta E_{\text{sens}} = m_{\text{redox}} \int_{T_{\text{start}}}^{T_{\text{end}}} c_{p,\text{redox}} dT.$$ (26)

The chemical energy for a reduction reaction is:

$$\Delta E_{\text{red}} = n_{\text{redox}} \int_{\delta_{\text{start}}}^{\delta_{\text{end}}} \bar{h}_{\text{r}}(\delta) \, d\delta$$ (27)

while for an oxidation reaction it is:

$$\Delta E_{\text{ox}} = \Delta E_{\text{red}} - n_{\text{ox}} \text{HHV}_{\text{syngas}}.$$ (28)

It is important to note that during reduction, a large temperature gradient across the redox material will cause a variation in the value of δ, which has been observed in experimental demonstrations.

The calculation of ΔE_{ins} is not straightforward, especially due to the transient behavior of the system which prohibits simple conduction calculations via the insulation. For accurate

determination from experimental data, a vast array of thermocouples must be placed in many locations to be able to calculate this term. This is impractical in most cases, due to the size and geometry of the inert parts in most solar redox reactors. The other option is to calculate it from the energy balance if all other terms can be calculated accurately from the experimental measurements. Usually, this term is lumped with the cooling water heat Q_{cw} since both are difficult to measure accurately. For a purely theoretical analysis, this term can also be estimated as a proportional term to ΔE_{sens}, with larger values for smaller reactors due to the unfavorable surface-to-volume ratio of such systems,

$$\Delta E_{ins} = f_{ins}\Delta E_{sens}, \tag{29}$$

with f_{ins} as the proportional term. Since in theoretical analysis, it is not straightforward to accurately calculate the heat terms (except the solar energy input and reradiation losses), the same method of using a scaling factor can be applied to include all of these losses. In fact, they are also dependent on the scale of the system and the surface-to-volume ratio. In this case we can write:

$$\Delta E_{other} = \Delta E_{ins} + Q_{conv} + Q_{rad} + Q_{cw} = f_{other}\Delta E_{sens} \tag{30}$$

The value of f_{ins} and f_{other} can be determined from experimental data (where available). In general, a larger system would have a better (lower) value.

We also note the following energy intensive processes that are directly related to the solar redox process: (a) heating of the oxidizer, which is critical in the case of water splitting; (b) heating of the inert sweep gas for such reactors; (c) the energy required for the separation of the outlet stream; and (d) in most cases, the required compression of the H_2 or syngas for downstream processes. In this work, we include (a) and (b), but leave (c) and (d), noting that this has to be accounted for in a complete solar fuel plant system analysis by considering these additional unit operations. The complete details of the calculation of all relevant energy terms are provided in the supplementary information.

3.1.2. Energy balance and reactor efficiency

By calculating all the energy terms, and including the auxiliary energy terms (pumping work, inert gas separation, inert/oxidizer heating) we can find the energy balance on the reactor and calculate the reactor efficiency (per Equation 5). The full calculation method is detailed in the supplementary information.

Table 3: General system parameters

Solar redox reactor (CeO$_2$ redox material)		
Reduction temperature T_{red}	1550	°C
Oxidation temperature T_{ox}	1000	°C
O$_2$ partial pressure (vacuum) p_{O_2}	1	mbar
O$_2$ mole fraction (sweep gas) x_{O_2}	10^{-6}	-
Concentration ratio C	2500	-
Other losses ratio f_{other}	0.3	-
Heat recovery effectiveness (redox material) ε_{HR}	0.4	-
Heat recovery effectiveness (gas-to-gas) $\varepsilon_{\text{HR,gas}}$	0.75	-
Oxidation extent α	0.95	-
Heat-to-work efficiency η_{hw}	0.4	-

The values chosen for the solar redox reactor parameters for the baseline case presented in Table 3 are based on the following data and assumptions: (a) T_{red} is limited to 1550 °C as a number of studies have reported concerns about CeO$_2$ sublimation at higher temperatures [82, 83]; (b) T_{ox} is chosen as sufficiently high to minimize the temperature swing while still allowing for high conversion extent; (c) p_{O_2} is selected as a value that is an order of magnitude lower than the reported values for the best demonstrations, thus assuming an improvement above the state of the art, while x_{O_2} is taken as the mole fraction in high-purity N$_2$; (d) the value of C is taken as the reported values in real on-sun demonstrations [10, 12], assuming it is feasible in a larger scale; (e) the value of f_{other} assumes an improvement over the demonstrated state of the art (0.42); (f) ε_{HR} assumes a realistic implementation which is well above the demonstrated state of the art (more details in subsection 3.2); (g) $\varepsilon_{\text{HR,gas}}$

31

is assumed, considering that these high temperatures are challenging for gas phase heat exchangers (consistent with [33, 32, 44]), and (h) the oxidation extent α is chosen to benefit performance as the reaction rate is the highest at the beginning of the oxidation step, but as it slows down, the penalties of heat losses, poor conversion extent, and more sensible heating of the oxidizer outweigh the benefits of complete oxidation [32].

The energy balance fraction terms in the following figures are: e_{fuel}: fuel energy (which is equal to η); e_{pump}: pumping energy; e_{exo}: exothermic heat; e_{rerad}: reradiation losses; e_{ox}: required oxidizer heating; e_{sens}: sensible redox material heating; e_{other}: other losses; e_{inert}: inert gas separation (sweep gas only); e_{heat}: required inert gas heating (sweep gas only).
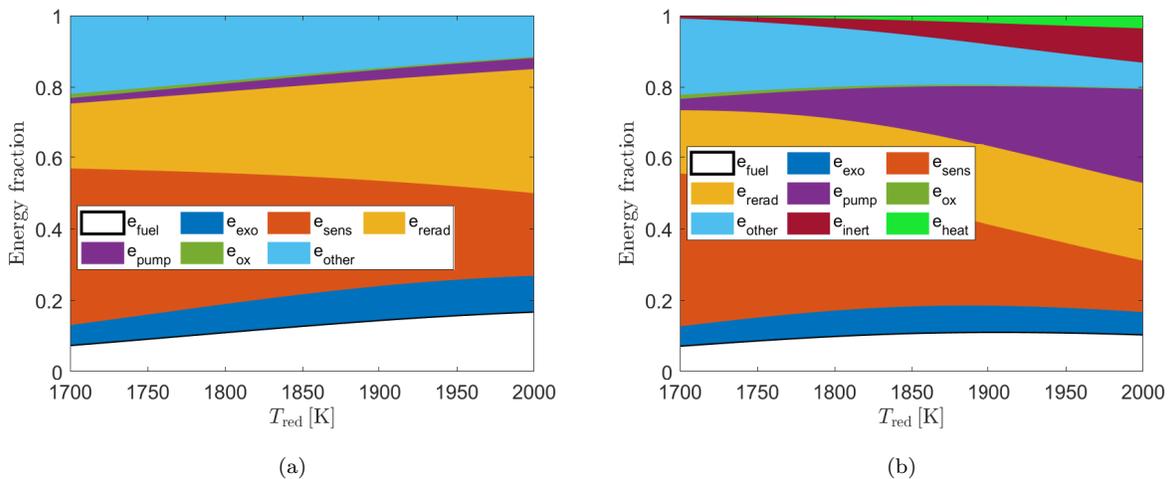
Figure 6: Reactor efficiency η and energy breakdown as a function of T_{red} for: (a) vacuum operated reactor, and (b) sweep gas operated reactor. The analysis performed for the baseline cycle (Table 3).

For the base case we calculate a value of $\eta = 12$ % and 10.5 % for vacuum and sweep gas operated reactors, respectively, with sensible redox material heating (35 % of Q_{solar}) and reradiation (24 % of Q_{solar}) as the largest energy losses. The effect of varying the reduction temperature is evaluated both for vacuum and sweep gas reactors (Figure 6). As expected from the thermodynamics of the system, increasing the reduction temperature is beneficial for the reactor efficiency in both types of reactors, increasing from $\eta = 7.5$ % at $T_{\text{red}} = 1700$ K to 16.9 % at $T_{\text{red}} = 2000$ K. More insight can be gained by looking at breakdown of the different energy terms as function of temperature. For the vacuum operated reactor (Figure 6a), it is clear that reradiation losses become the dominant energy term at high temperatures, limiting

the increase in reactor efficiency. Since the figure presents a normalized value, it is noted that both the redox material sensible heat as well as the other losses increase as well, however their share of the total energy balance is relatively constant. The pumping energy is increasing due to the increased reduction extent, with relatively more O_2 moles to be evacuated at lower pressures. When examining the behavior for sweep gas reactors (Figure 6b) we note a significant increase in the energy demand for the pumping and inert gas separation, resulting from the greater reduction extent. More O_2 moles released from the redox material at low partial pressures require larger amounts of sweep gas, thus decreasing the improvement in overall reactor efficiency compared to vacuum reactors. To a lesser extent, going to higher reduction temperature also increases the required inert sweep gas heat. The competing effects of increased $\Delta\delta$ with increased energy consumption result in η increasing from 7.3 % at $T_{\text{reduction}} = 1700$ K to 10.5 % at $T_{\text{red}} = 2000$ K, but with a maximum $\eta = 11.2$ % at $T_{\text{red}} = 1908$ K.
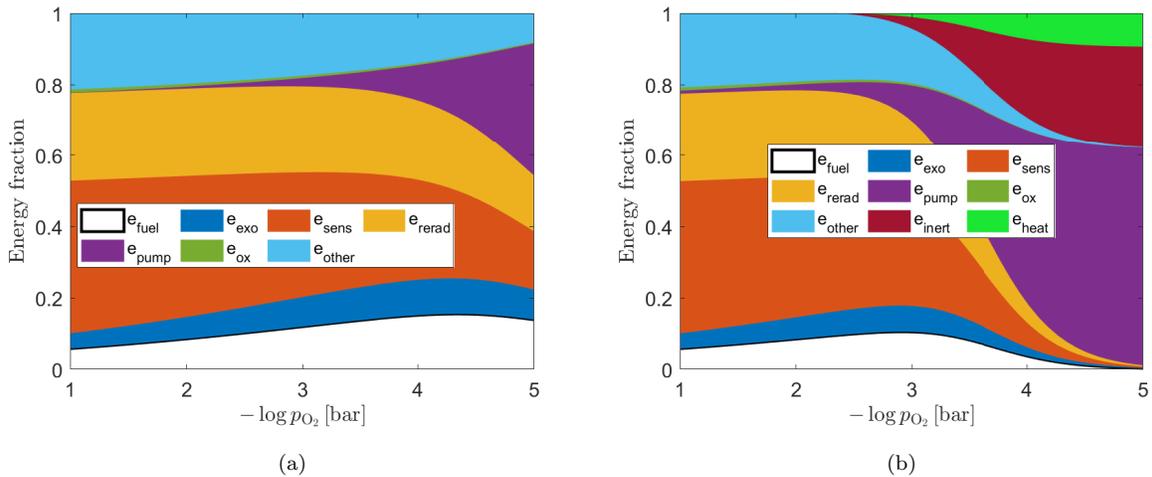

Figure 7: Reactor efficiency η and energy breakdown as a function of p_{O_2} for: (a) vacuum operated reactor, and (b) sweep gas operated reactor. The analysis performed for the baseline cycle (Table 3).

The effects of the O_2 pressure during reduction are plotted in Figure 7. While the pumping energy increases drastically for vacuum reactors, the benefits of greater reduction extent outweigh the additional energy demand until an optimal pressure is reached, as is shown on Figure 7a, with η increasing from 5.8% (at $p_{O_2} = 100$ mbar) to 15.5% (at $p_{O_2} = 0.045$ mbar). At lower pressures, the increase in pumping work exceeds the gain in reduction extent,

resulting in $\eta = 13.9\%$ at $p_{O_2} = 0.01$ mbar For sweep gas reactors, the efficiency peaks at 10.5% ($p_{O_2} = 1.33$ mbar), after which both the pumping energy and inert gas separation (and to a lesser extent, the sweep gas heating) drastically increase, lowering the overall efficiency.
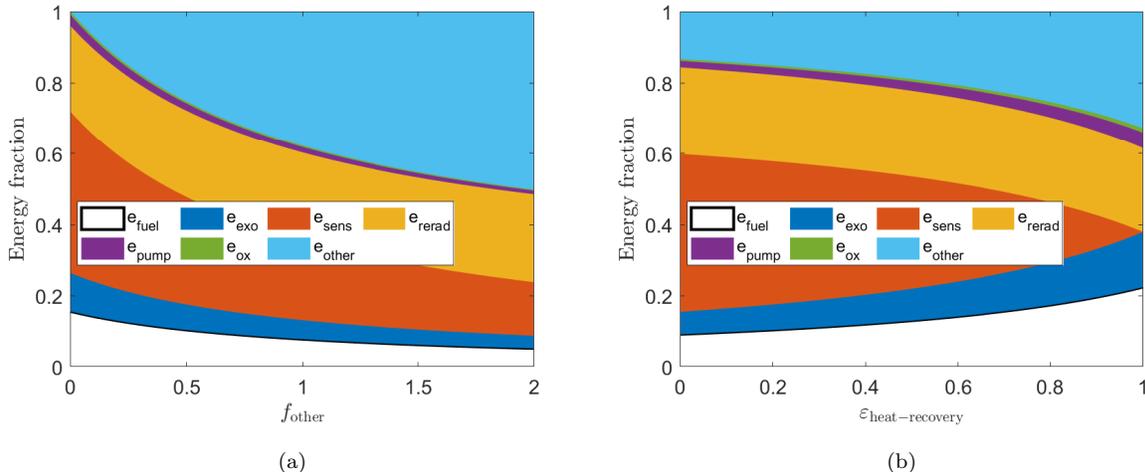

Figure 8: Reactor efficiency η and energy breakdown for a vacuum operated reactor as a function of (a) f_{other}, and (b) ε_{HR}. The analysis performed for the baseline cycle (Table 3).

For some of the parameters, the trends were identical for both vacuum and sweep gas reactors, with a slight advantage in terms of efficiency for the vacuum reactors. Hence, we include here only the figure for vacuum reactors (the complimentary figures for sweep gas reactors are in the supplementary information). When examining the effect of the other losses f_{other} (Figure 8a), the performance decreases with larger losses fraction as expected. However, it is important to note that even for an ideal reactor with $f_{other} = 0$, the reactor efficiency is just below 16% (taking into account quite optimistic values as per Table 3). In Figure 8b we show the effect of heat recovery on the energy balance and performance. While there is no surprise in the trend of improved performance with increased ε_{HR}, we note that the maximum reactor efficiency was 22.4% for perfect heat recovery (ε_{HR}). A more detailed analysis and discussion on the limitations of heat recovery as well as the cross effects of heat recovery and other losses is presented in subsection 3.2.

The effects of changing the temperature swing is presented in Figure 9a for a fixed T_{red}. Due to the assumed heat recovery effectiveness of both solid sensible heat and gas streams, there is a moderate improvement for higher oxidation temperatures, peaking at $\eta = 17.8$
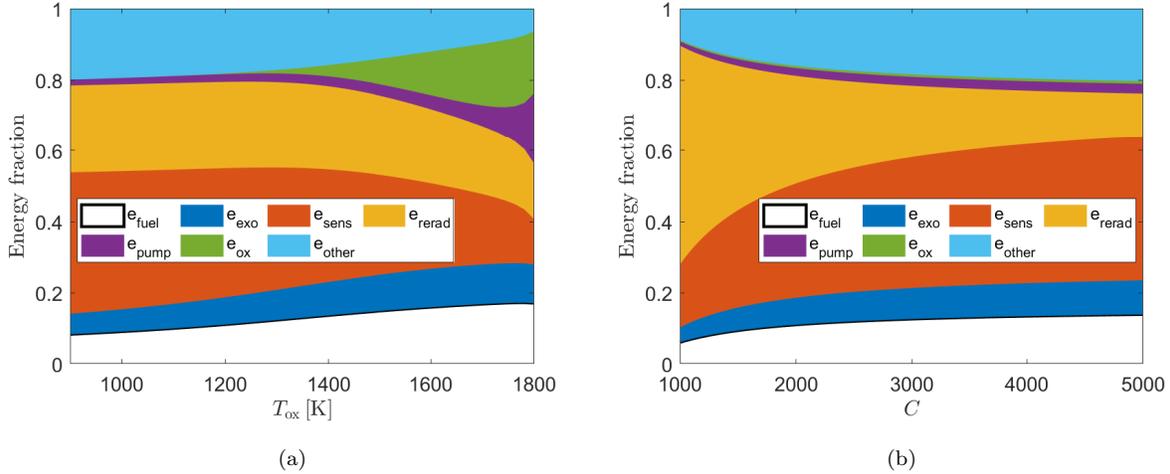
Figure 9: Reactor efficiency η and energy breakdown for a vacuum operated reactor as a function of (a) T_{ox}, and (b) C. The analysis is performed for the baseline cycle (Table 3).

% for $T_{ox} = 1782$ K, before dropping slightly due to the excessive oxidizer required for a near isothermal cycle. However, we do note that the conversion is lower for higher values of T_{ox}, which would lead to increased flow rates and additional energy requirements for product stream separation. While we assume here an isothermal oxidation step, in the demonstrations to date the exothermic reaction heat was insufficient in maintaining a constant reactor temperature [27, 28, 12, 11]. This might slightly change the trends, as the oxidation end temperature will be lower than its starting temperature. On the other hand, a better insulated reactor might stay at the same temperature or even experience a temperature increase due to the exothermic nature of the oxidation reaction. The effects of varying the concentration ratio are presented in Figure 9b. The improvement in performance is more significant over the lower concentration ratios, reducing the reradiation losses. While the maximum value of η is only increased to 13.9%, we examine later the combined effect of varying both T_{red} and C.

While efficiency maps have been generated for all the combinations of each two parameters ($T_{red}, T_{ox}, p_{O_2}, \varepsilon_{HR}, f_{other}, C$), we present here only the most interesting results. Several more efficiency maps are provided in the supplementary information. The effect of matching the reduction temperature to the O_2 partial pressure is plotted in Figure 10a. At lower reduction temperatures it was found that lowering p_{O_2} still improved efficiencies, while at higher
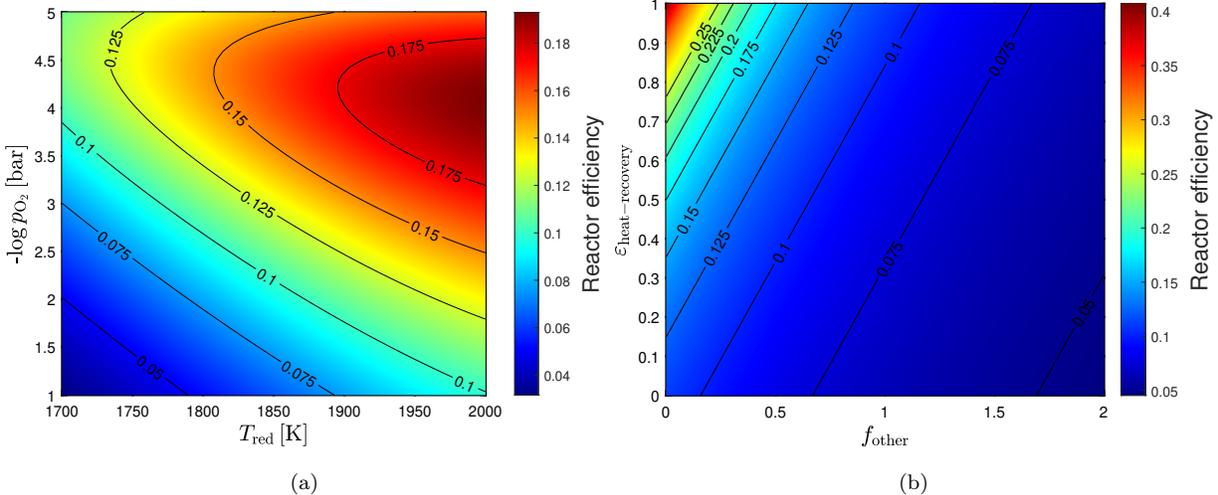
Figure 10: Reactor efficiency η for a vacuum operated reactor as a function of (a) T_red and p_{O_2}, and (b) f_other and ε_HR. The analysis is performed for the baseline cycle (Table 3).

temperatures the efficiency decreased above a specific pressure. This could be attributed in part to the lower pump efficiency—when a larger amount of O_2 needs to be pumped at lower p_{O_2}, the energy gains are smaller. It is clear that for each reduction temperature there is a corresponding optimal p_{O_2}, above which the efficiency starts to decrease, due to the larger amount of O_2 that needs to be pumped out of the system. From Figure 10b we can see the coupled effects of heat recovery and other losses. If our reactor is inefficient in terms of large inert mass and high losses, even a highly effective heat recovery system will not be able to increase its efficiency over 10%. This limitation is often overlooked, but it will present a significant hurdle for researchers attempting to demonstrate higher efficiencies using heat recovery at lab scale and small pilot systems.

The coupled effect of heat recovery and reduction temperature is presented in Figure 11a for a vacuum operated reactor. At higher reduction temperatures the improvement in the heat recovery becomes more dominant. It is clear that in order to achieve a reactor efficiency over 10%, a combination of both is required. Implementing heat recovery alone while keeping the reduction temperatures low is highly unlikely to yield significant improvements. We also present the coupled effects of the reduction and oxidation temperatures on the reactor efficiency for a sweep gas operated reactor (Figure 11b). We show here that increasing the reduction temperature improves the performance for an oxidation temperature below

36
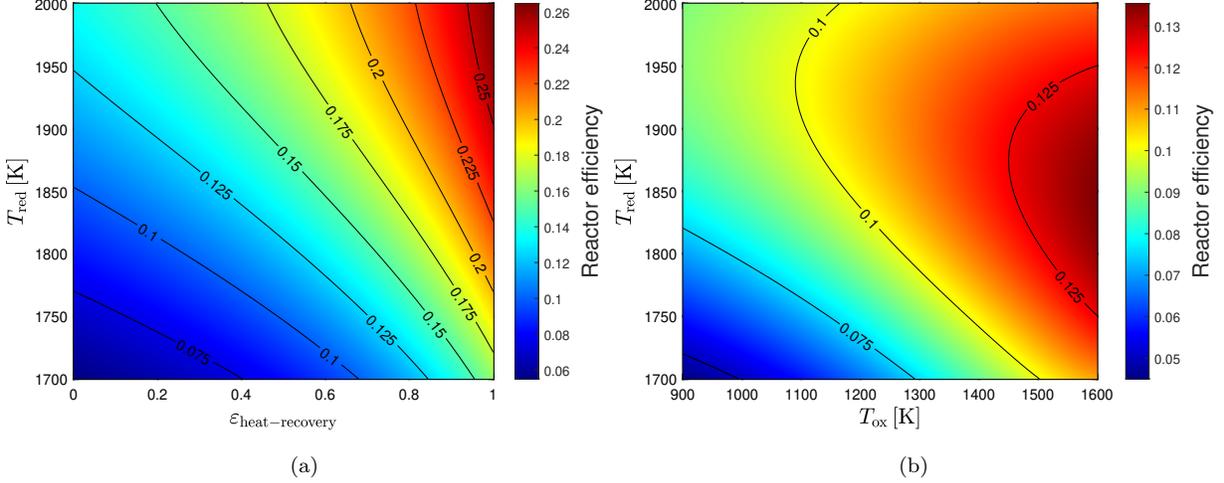
Figure 11: Reactor efficiency η as a function of (a) ε_{HR} and T_{red} for a vacuum operated reactor, and (b) T_{ox} and T_{red} for a sweep gas operated reactor. The analysis is performed for the baseline cycle (Table 3).

1100 K, but above this threshold, the trend begins to change, with a decrease in efficiency for $T_{red} > 1950$K for the higher oxidation temperatures (>1250 K). This is attributed to the larger energy required to purify the inert gas and preheat it, overtaking the extra energy for the oxidizer preheating. We note that both gas streams assume the same $\varepsilon_{HR,gas}$.

Summarizing these results, it is evident that any realistic solar reactor is limited to lower efficiencies than is predicted in the various theoretical studies. With optimistic assumptions of heat recovery effectiveness of 75% and 40% for the gas-gas and redox material, respectively, reactor efficiencies over 15% require higher reduction temperatures and lower O_2 partial pressures than has been applied to date in demonstrations. In addition, minimizing the other losses (f_{other}) is another important avenue, requiring new reactor design concepts. However, any solar reactor operating in a cyclic batch mode at these high temperatures would inevitably incur such heat losses. Increasing the insulation to such a degree that will minimize the losses to the ambient will increase the transient heating/cooling losses, as well as require extremely long duration of preheating until the system reaches a steady cyclic mode (i.e., the state in which each cycle is identical to the previous one) due to the larger thermal mass. These are all important design questions, which should be carefully analyzed, in order to choose an effective design strategy. Having said that, the possible gains in efficiency over the state of the art are likely to be in single digits, at least for fixed bed cavity-type reactors.

3.2. Heat recovery limitations

The sensible heating of the redox material and inert reactor parts has been identified as the largest parasitic loss of solar thermochemical fuel production, owing to the large temperature difference required for temperature-swing solar redox processes [27, 12, 84]. In some cases, the sensible heating of the redox material and inert parts accounted for more than 50% of the total solar energy input [27]. In an isothermal redox cycle, on the other hand, no heat recovery from the redox material is possible or needed due to the constant operating temperature, but achieving practically relevant feedstock conversion extent is a challenge. Both types of reactors (temperature-swing and isothermal) could benefit from gas-gas heat recovery during the oxidation step, as well as during the reduction step for sweep gas operated reactors. While still operating at high temperatures, this type of heat transfer is more easily implemented and can achieve high effectiveness and minimize some of the parasitic losses such as sweep gas and oxidizer preheating [26, 37]. Lastly, sensible heat recovery has been one of the largest motivations for the development of moving redox material systems [23, 24, 85, 86, 57, 87, 55, 88]. However, as discussed in other parts of this manuscript, this approach requires overcoming significant technical barriers. A more comprehensive list of different heat recovery concepts could be found in the work of Lidor *et al.* [84].

Actual demonstrations of solar reactors with a solid heat recovery systems are rare, with only a few published studies. The first demonstration of such a system was the CR5 reactor [23], composed of counter-rotating rings with solid-solid heat recovery. The reactor operated for over an hour on-sun, but suffered from material stability issues due to moving parts at high temperatures. A modified version, using CeO_2 as the redox material and including design improvements [24] was able to operate longer, but still resulted in poor performance and mechanical failures that have been identified after only a few runs. A concept for high-temperature heat recovery using two thermocline-based thermal energy storage (TES) units with a reactive zone and coupled to a solar receiver for an indirectly heated redox cycle has been proposed, dubbed as the dual-storage reactor [15]. This method was experimentally demonstrated using electric heaters embedded within the TES units. While heat recovery effectiveness values of 33-52% were reported, the thermal mass (mc_p) of each

TES unit was more than 600 times larger than the thermal mass of the redox material, making the results of little practical relevance. Another approach called the dual heat storage system was proposed, using a directly irradiated cavity-type solar reactor and separate TES units [84]. In this concept, an inert HTF was used to extract the high-temperature heat from the redox material and charge a TES unit. This heat could later be recuperated into the reactor after oxidation, preheating it before reduction is resumed with concentrated solar radiation. The system was tested in a high-flux solar simulator, but due to the heat losses between the reactor and TES units, attributed to the unfavorable surface-to-volume ratio and large thermal mass of the piping and valves, the TES charging temperature was too low to allow recuperation, but up to 70% of the heat was successfully extracted from the reactor at temperatures up to 1300 °C. An attempt to demonstrate only the heat recovery, without any redox reaction, was followed by placing the TES as close to the reactor outlet as possible [89]. With this setup, a heat recovery effectiveness of 33% was achieved with an HTF temperatures up to 1100 °C, based on the HTF temperature reintroduced into the reactor. Additionally, several limitations of this concept have been discussed, with possible approaches to improve the design.

The heat recovery effectiveness is defined as the ratio between the useful sensible heat introduced or recuperated back into the redox material at the end of a cycle, compared to the required sensible heat for increasing the redox material temperature from oxidation to reduction temperature:

$$\varepsilon_{\text{HR}} = \frac{Q_{\text{recovered}}}{Q_{\text{sens}}} = \frac{m_{\text{redox}} \int_{T_{\text{ox}}}^{T_{\text{HR}}} c_p}{m_{\text{redox}} \int_{T_{\text{ox}}}^{T_{\text{red}}} c_p}, \tag{31}$$

with T_{HR} being the maximum obtained temperature of the redox material due to heat recovery. A solar receiver-reactor, whether integrated in a single device or split into a solar receiver and redox reactor, has a large thermal mass. When considering heat recovery, two extreme cases could be considered: (a) sensible heat is recovered from the redox material only; (b) sensible heat is recovered from the redox material as well as from the inert reactor parts. The performance of any practical system must lie between these two extremes.

3.2.1. Heat recovery assuming only redox material heat

Here we analyze the effect of heat recovery on the reactor efficiency for the case where it is assumed sensible heat is recovered only from and to the redox material. We define the ratio of the redox material sensible heating required to the solar energy input as:

$$f_{\text{sens}} = \frac{\Delta E_{\text{sens}}}{Q_{\text{solar}}}. \tag{32}$$

with ΔE_{sens} defined in Equation 26. We can calculate the reactor energy efficiency with heat recovery:

$$\eta_{\text{with-HR}} = \frac{n_{\text{fuel}}\text{LHV}_{\text{fuel}}}{(1 - \varepsilon_{\text{HR}})\Delta E_{\text{sens}} + \Delta E_{\text{red}} + \Delta E_{\text{ins}} + Q_{\text{loss}} + Q_{\text{rerad}} + W_{\text{aux}}} \tag{33}$$

with ε_{HR} as the heat recovery effectiveness per Equation 31. We divide this term by the standard definition for η (Equation 5). Assuming $Q_{\text{solar}} \gg W_{\text{aux}}$ we get the ratio of improvement in the reactor efficiency due to heat recovery:

$$\frac{\eta_{\text{with-HR}}}{\eta} = \frac{1}{1 - f_{\text{sens}}\varepsilon_{\text{HR}}}. \tag{34}$$

From this, we can see that increasing the value of ε_{HR} is beneficial for increasing η, as expected. However, it is clear that for heat recovery to have a significant effect, the value of f_{sens} must be high as well. In practical terms, it means that the sensible heat of the redox material must consist of a significant part of the required solar energy input, i.e. that all other losses and parasitic terms, such as the insulation required energy, must be relatively small. The results are presented in Figure 12a.

From the figure it is clear that even a perfect heat recovery will not double the efficiency to values exceeding 10% for the best demonstrated reactors. This is due to the simple fact that all other energy terms (reradiation losses, losses from the reactor shell, transient heating/cooling of the inert parts, etc.) are unaffected by heat recovery from the redox material. So, only a single, even if significant, energy term is being mitigated. A theoretical reactor with $f_{\text{sens}} = 0.5$ (50% of the solar energy is used to heat up the redox material), an

extremely high value, could reach a factor of 2 improvement only with perfect heat recovery, a feat that is unfeasible (dotted line in Figure 12a).

This calculation can be viewed as the conservative estimation of heat recovery since it assumes that only sensible redox material heat is recovered. In the next subsection we calculate another case, in which heat is recovered from both the redox material and inert reactor parts.

3.2.2. Heat recovery assuming redox material and insulation heat

Here we follow a similar approach for the previous case of sensible heat recovery from the redox material only, but we add the recovery of sensible heat from the inert parts (insulation). The ratio of the redox material and insulation sensible heating required over the solar energy input is:

$$f_{\text{sens,comb}} = \frac{\Delta E_{\text{sens}} + \Delta E_{\text{ins}}}{Q_{\text{solar}}}. \tag{35}$$

with ΔE_{ins} defined per Equation 29. The rest of the following mathematical development is identical to the one for the previous case. We can calculate the reactor efficiency with heat recovery per:

$$\eta_{\text{with-HR}} = \frac{n_{\text{fuel}}\text{LHV}_{\text{fuel}}}{(1 - \varepsilon_{\text{HR}})(\Delta E_{\text{sens}} + \Delta E_{\text{ins}}) + \Delta E_{\text{red}} + Q_{\text{loss}} + Q_{\text{rerad}} + W_{\text{aux}}} \tag{36}$$

and by using the term from Equation 35 we get:

$$\frac{\eta_{\text{with-HR}}}{\eta} = \frac{1}{1 - f_{\text{sens,comb}}\varepsilon_{\text{HR}}}. \tag{37}$$

As in the previous section, we can see that increasing the value of ε_{HR} is beneficial for increasing the η. This case can be considered the most ideal case since we assume that the heat recovery is effective both for the redox material and inert parts' sensible heat in the same manner. The realistic value must lie somewhere between these two extremes. Since the sensible heat of the insulation is probably not recovered with the same effectiveness as the redox material sensible heat, and also should be minimized in an ideal reactor, the approach

shown before could be extended to a case with two different parameters, f_{sens} (as in eq. 32) and $f_{\text{ins}} = \Delta E_{\text{ins}}/Q_{\text{solar}}$, and two different heat recovery effectiveness values $\varepsilon_{\text{HR,sens}}$ and $\varepsilon_{\text{HR,ins}}$, to yield the following:

$$\frac{\eta_{\text{with-HR}}}{\eta} = \frac{1}{1 - f_{\text{sens}}\varepsilon_{\text{HR,sens}} - f_{\text{ins}}\varepsilon_{\text{HR,ins}}}. \tag{38}$$

The results are plotted in Figure 12b. The theoretical reactor in this case assumes the same $f_{\text{sens}} = 0.5$ and a lower $f_{\text{ins}} = 0.25$ for the fraction of the various inert parts heating. While this might seem high, this in fact increases the potential for high efficiency improvement (lower f_{ins} means less heat could be recovered from the inert parts). We use it as the optimistic upper bound, contrary to the conservative case. For the demonstrated solar reactors, the most ideal case of perfect heat recovery of the redox material and inert parts sensible heat still results in values of $\eta_{\text{with-HR}}/\eta < 2.5$. These unrealistically high values would still amount for η of 12.9% and 9.86% for the Marxer *et al.* reactor and Zoller *et al.* reactor, respectively. The theoretical reactor could reach a factor of 4 improvement for perfect heat recovery, which is significantly higher. For realistic values of ε_{HR}, a factor of 2 could be obtained.

3.2.3. Thermodynamic limits on heat recovery in stationary temperature-swing reactors

In previous works considering heat recovery [53, 79, 81, 44], a wide range of values for the heat recovery effectiveness is chosen up to a value of $\varepsilon_{\text{HR}} = 1$ for a perfect heat recovery. If we consider heat recovery from a solar reactor operating in a cycling process, between reduction and oxidation, there are some inherent limitations that must be taken into account: (a) the heat is recovered at variable temperature, starting from the highest value T_{red} to the lowest value T_{ox}; (b) the heat must be stored in some manner, ideally keeping its quality high by implementing a temperature profile; and (c) heat recuperation into the reactor is also a transient process, with ΔT changing as the redox material is being heated from T_{ox} towards T_{red}.

Let us consider a case, in which we assume heat is extracted from a solar reactor at the end of reduction, stored, and reused after oxidation. We focus on the demonstration of a specific heat recovery method of using an inert HTF with a stationary volumetric solar reactor, such as in Lidor *et al.* [84, 89], however it is applicable to any method of sensible heat recovery from
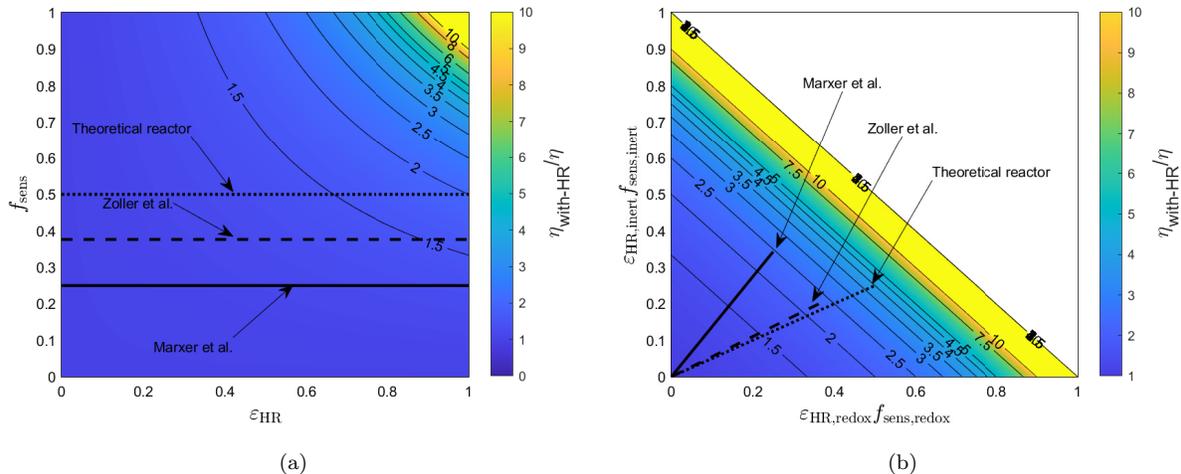
Figure 12: Ratio between reactor efficiency with heat recovery to the reactor efficiency without heat recovery: (a) heat recovery from sensible metal oxide heat only, and (b) heat recovery from sensible heat of metal oxide and inert reactor parts. The yellow area above $\eta_{\text{with-HR}}/\eta = 10$ is increasing exponentially and has been capped, since it is impractical to achieve such high values in real systems. The white area represents non-physical results (sum of energy fractions over 1). The theoretical reactor is a reactor with $f_{\text{sens}} = 0.5$ and $f_{\text{ins}} = 0.25$.

a fixed bed reactor using an HTF and a sensbile heat TES. We assume no heat losses from the solar reactor during heat extraction (and no heat conducted from the redox material to the insulation), negligible energy/exergy in the fluid remaining in the reactor, and neglecting the entropy change of the redox material during heat extraction, to calculate an upper boundary exergy efficiency. Assuming $T_1 = 1823$ K (reduction temperature), $T_2 = 1223$ K (oxidation start temperature), $T_{\text{ref}} = 973$ K (oxidation end temperature), and $t_{\text{extraction}} = 360$ s we get a value of $\eta_{\text{2nd,extraction}} = 0.726$. In practical terms, it means the quality of the heat degrades and its usefulness in high-temperature heat recovery is diminished. We also note that this degradation in heat quality is for the heat extraction only—coupled with the inherent irreversibilities in the heat storage and heat recuperation of the stored heat into the reactor, it is clear that the practical limitations of heat recovery in such systems is significantly lower than a perfect heat recovery of $\varepsilon_{\text{HR}} = 1$.

In theory, if a method could be developed for extracting the heat from a stationary redox material in a solar reactor at infinitesimally small quantities, storing each heat extracted separately (to avoid mixing between heat storage media at different temperatures) in an

adiabatic container, and reintroducing the heat back into the reactor at the correct order (starting from $T = T_\text{ox} + \Delta T$), perfect heat recovery could be obtained. Of course, such a process is not feasible with real systems, and would take infinite amount of time.

Using a thermocline-based TES system [90, 84, 89, 48] could partially utilize the fact that heat is stored at different temperatures. Using thermocline control methods might slightly mitigate the thermocline degradation further [91, 92]. However, the fact that the highest-temperature heat is extracted first and that the TES charging temperature is decreasing inherently causes a thermocline degradation. Coupled with the technical challenges such as heat losses and thermal inertia, exceeding a value of $\varepsilon_\text{HR} = 50\%$ in such a thermocline-based heat recovery system is highly unlikely. Of course, using counter-current systems and performing direct solid-solid heat recovery are not limited by these constraints, and have been a topic of theoretical study [57, 87, 88]. However, such systems are yet to be experimentally demonstrated, and the technical challenges associated with moving high-temperature redox materials while keeping inert or vacuum atmospheres are very significant.

The use of a thermochemical energy storage for heat recovery might merit more research, since if a suitable thermochemical reaction is identified with high enough exothermic reaction temperature, a stable heat recovery temperature could be used [93]. However, this approach would require a complex heat recovery system, basically adding another set of chemically reactive species to handle in the process.

Another approach that might hold more promise is using a hybrid approach of sensible heat recovery coupled with electrical heating for upgrading the quality of the heat, such as used for trace heating in molten salt CSP plants. Depending on the specific design, embedding electrical heaters in the system might provide the necessary boost to upgrade the heat to useful temperatures, at relatively low energetic costs. Alternatively, the heat could be extracted from the redox material following reduction and used in a separate process, such as a power block or as high-quality process heat. Due to the simpler requirements for moving and storing the heat in this case, a higher combined reactor efficiency for both syngas and heat output could be achieved (see supplementary information for more details and results). Since the extraction of the heat was already demonstrated at effectiveness up to 70% [84], this combined approach is certainly feasible and merits further study.

44

If the use of multiple reactors is envisioned [94, 10], directly extracting the heat from the reduced reactor into an oxidized reactor might mitigate some of the losses, allowing to get closer to the thermodynamic limit. Still, this implies that a near perfect control and operation of the system could be developed to minimize the idle wait time of each reactor and increase the solar utilization [95]. Longer idle times will translate to longer cycle duration and lower power output densities.

Lastly, it is important to note that heat recovery might add two additional steps into a temperature-swing solar reactor: the heat extraction and heat recuperation. While the heat extraction might have a positive effect by shortening the cycle duration due to faster cooling compared to passive cooling, heat recuperation under small temperature difference will be slow, and might extend the overall cycle duration [90]. Combined with the fact that it adds additional heat exchange and storage equipment, this could significantly decrease the overall power density, which is already a critical issue for these systems.

3.3. Real reactor limitations summary

The analysis presented incorporates fundamental thermodynamics with practical system limitations for a CeO_2-based system, allowing us to develop performance maps for solar redox reactors under a wide range of parameters. Some previous works predict reactor efficiencies over 20% for moderate operating conditions ($T_{red} \leq 1500$°C), using various assumptions on the heat losses (or lack of), lowering the p_{O_2}, or applying highly efficient heat recovery [53, 79, 80]. In our analysis, we conclude that a modest reactor efficiency of approximately 12% is a more realistic goal, while still requiring challenging technical solutions for high-temperature heat recovery and reactor design.

4. Scale-up analysis

In subsection 1.1 we have shown the power density of several prominent experimental demonstrations. We now expand upon this, to calculate the potential power density of solar thermochemical fuel production, as well as analyze several other parameters that are critical for sizing and scaling-up these systems. For the sake of clarity, we use here $\eta_{reactor}$ for the reactor efficiency, to distinguish between the other efficiencies. All the results are for

vacuum operated reactors, as they exhibited superior performance. An upper-bound on the volumetric power density and specific power of a solar reactor system can be calculated from:

$$\text{Volumetric power density} = \frac{P_{\text{out}}}{V_{\text{reactor}}} = \frac{\rho_{\text{redox}}\left(1 - \varepsilon_{\text{void}}\right)\Delta\delta \text{HHV}_{\text{syngas}}}{M_{\text{redox}}t_{\text{cycle}}} \tag{39}$$

$$\text{Specific power} = \frac{P_{\text{out}}}{m_{\text{redox}}} = \frac{\Delta\delta \text{HHV}_{\text{syngas}}}{M_{\text{redox}}t_{\text{cycle}}} \tag{40}$$

with $\rho_{\text{redox}}\left(1 - \varepsilon_{\text{void}}\right)$ as the effective redox material density. We note that this upper-bound does not include insulation, reactor housing or auxiliary equipment, which can add significantly to the size of these systems. For example in most demonstrations, the vacuum pump is much larger than the reactor, due to the large volumetric flow rates at low pressure.

For a system with CeO_2 as the redox material and high density ($\varepsilon_{\text{void}} = 0.5$), assuming $\Delta\delta = 0.04$ and a cycle time of 30 min, we receive a power density of $133\,\text{kW}\,\text{m}^{-3}$ and specific power of $37\,\text{W}\,\text{kg}^{-1}$, excluding any dead space for a cavity or any containing shell/insulation. Increasing $\varepsilon_{\text{void}}$ and t_{cycle} to 0.7 and 60 min respectively, which corresponds to the values in previous demonstrations (and still excluding the cavity space), results in a power density of $40\,\text{kW}\,\text{m}^{-3}$ and specific power of $18.5\,\text{W}\,\text{kg}^{-1}$. The only possible methods to increase the power density for the CeO_2-based cycle are shortening the cycle duration (by increasing the solar power input, decreasing the temperature swing, or lowering the re-oxidation extent, as the oxidation reaction rate decays fast after its initial peak), increasing the reduction extent (lowering p_{O_2} and increasing T_{red}), and lowering the redox material void fraction (while keeping the surface area sufficiently high). It is also important to note that the reactor efficiency plays no role in the power density, although it can be assumed that an efficient reactor will exhibit higher $\Delta\delta$. Still, it explains why a less efficient reactor such as [26], but with smaller void fraction and shorter cycle duration, was able to achieve the best power density from all demonstrated systems.

We examine the full potential of the process power density as a function of $\Delta\delta$ and t_{cycle}, for a fixed case of using CeO_2 and with $\varepsilon_{\text{void}} = 0.5$, as plotted in Figure 13. These upper-bounds on power densities also apply to moving particle reactors, where the cycle time is
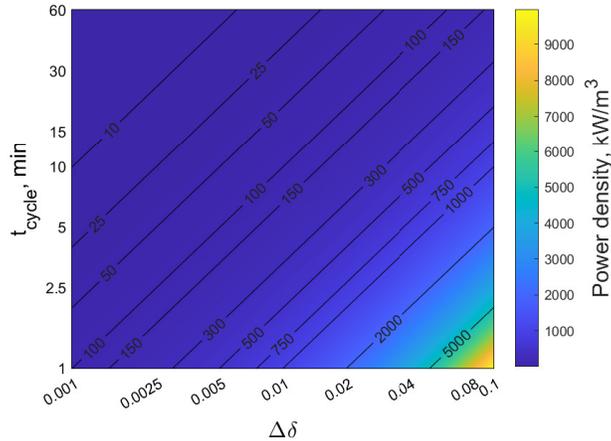
Figure 13: Power density as a function of $\Delta\delta$ and t_{cycle} for CeO_2 with $\varepsilon_{\text{void}} = 0.5$.

then the average time it takes a particle to move through the whole cycle. We set a minimum cycle time of 5 minutes and reduction extent of 0.01. Reducing the cycle duration should be a critical goal for further development, since at $t_{\text{cycle}} = 60$ min it is impossible to achieve power densities over $100\,\text{kW}\,\text{m}^{-3}$ without going to an extremely high reduction extent.

4.1. Scale-up analysis case study

We finish this part with an estimation of the scale-up of the technology for the production of aviation jet fuel (Jet A-1) via Fischer-Tropsch synthesis. We use the data in Table 3 and Table 4 to perform an annual production analysis for $4.11 \cdot 10^6$ m^3 of jet fuel. For context, that is 1% of the global annual production [96], 3.9% of the U.S. annual production [97], or less than a third of the Lufthansa group annual fuel consumption [98] (for 2019).

We define the overall system efficiency as:

$$\eta_{\text{system}} = \eta_{\text{opt}}\eta_{\text{reactor}}\eta_{\text{syngas-to-fuel}} \tag{41}$$

with η_{opt} as the heliostat field optical efficiency, η_{reactor} the reactor efficiency (per Equation 5), and $\eta_{\text{syngas-to-fuel}}$ as the fuel synthesis unit energy efficiency. We assume an ideal full conversion of syngas to jet fuel. The syngas to fuel efficiency only accounts for the loss in heating value due to the exothermic FT-process. Balance-of-plant operations such as separation and compression units are not accounted for, and would increase the overall energy requirement

Table 4: System parameters for scale-up analysis

Syngas synthesis process - (Fischer-Tropsch to Jet A-1 fuel)		
Syngas-to-fuel energy efficiency $\eta_{\text{syngas-to-fuel}}$	0.7	-
Syngas H_2:CO ratio	2	-
Fuel heating value LHV_{fuel}	43.24	MJ kg^{-1}
General process parameters		
Solar capacity factor f_{cap}	0.25	-
Optical efficiency η_{opt}	0.6	-
Cycle time t_{cycle}	60	min
Packed bed void fraction $\varepsilon_{\text{void}}$	0.5	-
Annual fuel production $V_{\text{fuel,annual}}$	$4.11 \cdot 10^6$	m^3

of the plant. The solar capacity factor is the fraction of the year at which that plant operates (full calculation details are provided in the supplementary information). For the input of the solar fuel plant analysis, we have used the data in Table 3 and Table 4 (unless specified otherwise).

For this analysis we define three cases:

- **Case 1:** the baseline case with all input parameters per Table 3 and Table 4. This is considered an optimistic case, since several improvements above the state of the art are assumed.

- **Case 2:** an ideal case, using the near-term future values from Moretti *et al.* [48]: $\eta_{\text{opt}} = 0.65$, $\eta_{\text{reactor}} = 0.3$, $T_{\text{red}} = 1500$ °C, and $p_{O_2} = 10$ mbar. We neglect the additional solar receiver penalty (0.65 in Moretti *et al.*) and DAC energy requirements. This is a very optimistic case, requiring many significant improvements above the state of the art.

- **Case 3:** a modified baseline case, taking all the input parameters from Table 3 and Table 4 except two operational parameters for the reduction: $T_{\text{red}} = 1700°\text{C}, p_{O_2} =$

0.1 mbar. This case examines the effect of these parameters only as an alternative development path to *Case 2*.

Table 5: Results for the annual production of a solar fuel plant.

Parameter	Case 1	Case 2	Case 3	
Reactor efficiency	11.9	30	19	%
System efficiency	5.01	13.7	7.96	%
Volumetric power density	57.3	24.9	217	$kW\,m^{-3}$
Specific power	15.9	6.9	60	$W\,kg^{-1}$
Cycled CeO_2 mass per fuel volume	919	2031	243	$kg\,L^{-1}$
Annual production of $4.11 \cdot 10^6$ m^3 of Jet A-1				
Required redox material mass	1724	3812	456	kt
Required solar energy	793	291	499	TWh
Required installed solar power	362	133	228	GW

The results for all cases, both for the specific properties and for the annual plant performance, are presented in Table 5. It is evident that for case 1 (base case), significant technological hurdles exist. Due to the low volumetric and specific power density, massive quantities of redox material must be cycled per unit of fuel produced. In addition, the required solar energy and power, delivered at high concentration, would create additional challenges.

To put the numbers for scale-up into some better context, consider *Case 1*, implemented with tower systems each having a 10 MW output power (in syngas heating value). Each tower would need multiple reactors operating in parallel to continuously utilize the concentrated solar energy. The total reactor volume for such a tower would need to be 175 m^3 with a total of 630 t of CeO_2. This huge net volume of the reactors needs to be vacuum tight and remain so during high-temperature cyclic operation. Assuming that such systems could be constructed, meeting 1% of current global aviation fuel demand would require 2600 towers, with a total heliostat area of $380\,km^2$ (assuming an annual direct normal irradiance (DNI)

49

equivalent to Daggett, CA of $2800\,\mathrm{kW\,h\,m^{-2}}$). The total mass of CeO_2 required to fill all the reactors would be more than 10 times the current global annual production of CeO_2 (108.92 kt per annum [99]).

These numbers do not make for a promising outlook for the scale-up of this technology. It is also worth noting that *Case 1* assumes several significant performance improvements over the state of the art, such as successful heat recovery (both for solid and gas, allowing for $\eta_{\mathrm{reactor}} > 10\%$), high optical efficiency for high concentration solar fields, and long-term operation stability of the reactors, none of which are a given.

Case 2 presents an ideal case as it is envisioned in the field, i.e. highly efficient components operating at more moderate conditions ($T_{\mathrm{red}} = 1500$ °C and $p_{O_2} = 10$ mbar). It can be seen from the results that while this case exhibits the lowest energy and power requirements compared to *Case 1*, the power density is less than half and the amount of required ceria and reactor volumes would be more than doubled.

Case 3 examines an alternative development strategy, which pushes the operational parameters of the solar reactor during reduction to higher temperature and lower oxygen pressures, while keeping all other parameters the same as *Case 1*. This approach can increase the efficiency, but crucially also improves the power density, which greatly improves the outlook for scale-up in terms of reactor volumes and CeO_2 mass requirements.

The high energy and power requirements, combined with the challenges of high-flux high-temperature solar fields [100], merit a cautious assessment on the scale-up of this technology. An interesting point is to identify the possible relevant scale of such a plant, considering the economic scaling of all subsystems: CST, redox reactor, and GTL.

4.2. Scale-up analysis summary

The low power density in the state-of-the-art CeO_2-based process is a serious hurdle to scale-up. It arises due to the semi-batch cyclic nature and the thermodynamic limitations on oxygen storage in CeO_2. As a result, extremely large quantities of redox materials must be cycled in the reactor to allow for any significant fuel production. The coupling of reactors in the size of hundreds of m^3 to a concentrated solar radiation source will present a serious technical hurdle for further development. This is reflected in the demonstrated state of the

art, where despite the testing of quite large reactor systems, the power output has yet to exceed a kilowatt.

5. Outlook

From the state of the art, and the thermodynamic and scale-up analysis performed here, it is clear that there are significant drawbacks to this technology, both its current performance and potential performance. From a purely energy conversion perspective it is unlikely to come close to the performance of PEM electrolysis systems coupled to renewable electricity. The basic principles of a heat to chemical work cycle require a very challenging combination of high temperature (see section 2) and cyclic batch or semi-batch operation, which has proven extremely difficult to develop. The challenge is further compounded by the recent stalling in deployment in the base CSP technologies. With these points in mind it is certainly worth reflecting on the challenges faced by this technology and how they might be overcome.

One drawback highlighted in this study that has not been discussed in detail to date, is the low volumetric and specific power density of the state-of-the-art processes. Even in the highly optimistic efficiency cases often assumed in the literature, the low power density would still present a major challenge for scale-up. Significantly improving the power density will be challenging for temperature swing cycles. Future research should take a broader view of performance and connect the dots between lab-scale experiments and how this would be reflected in a scaled-up system.

There are several future development options being considered within the field that aim to improve the overall performance including; 1) incrementally improving the state-of-the-art using for example heat-recovery, 2) changing the process design away from packed-bed temperature swing reactor systems to moving oxide systems or isothermal operation, 3) using alternative materials to CeO_2. However, there is currently little consensus as to which approaches are most promising, particularly in terms of changing the process configuration. Here we try to offer some outlook on these alternative development pathways.

There is also a clear *catch-22* in selecting the process conditions for this technology. From the basic principles of the heat to chemical work cycle, increasing the reduction temperature and decreasing the O_2 partial pressure during reduction are the most straightforward methods

for a significant improvement in the reactor efficiency and overall performance. However, lowering the O_2 partial pressure significantly below 1 mbar could be very challenging due to the volumetric flow rate increasing inversely with the pressure, leading to very large (and expensive) pumps. Similarly, most of the field are trying to move towards lower temperatures, due to the very challenging design constraints that the high temperatures present. However, while operating at milder conditions eases some of the engineering challenges related with these systems, it sabotages the primary function, which is the heat to chemical work cycle. There is unfortunately no simple answer here, leading to a lack of consensus in the field on the future development in regards to this trade off.

One well established avenue of further investigation is the decoupling of the solar receiver from the chemical redox reactor. These two functions often have conflicting requirements, and trying to design a device that performs both functions must compromise on one or both aspects. For example, the open cavity design requires the reactor to be mostly empty volume, which significantly decreases the power density. Designing a high-temperature solar receiver to deliver high-temperature heat to a separate packed-bed redox reactor may prove beneficial for performance, as well as separating the challenges associated with each component. A conventional packed bed-reactor can also benefit from alternating countercurrent flows between each cycle step, improving the outlook for performance in terms of feedstock conversion [101, 102]. Furthermore, a separated reactor and receiver approach could work well in a combined fuel and power production plant, where waste heat from the thermodynamic cycle could be used for power production [103]. Given the challenges of heat recovery within the cycle, this approach can offer a much more practical method of recovering and utilizing the sensible heat and the exothermic reaction heat from the cycle. While the heat to fuel efficiency would likely be limited, the overall plant design would become more pragmatic and could be effective for combined fuel and power production. On the downside there are a lot of significant challenges in developing receivers and heat transfer systems that can operate at the required high temperatures. This route is therefore not a simple or guaranteed solution.

Such decoupling of the solar receiver from the chemical reactor could also allow for a hybrid thermal-electrical system, using CST heat at temperatures of a few hundred degrees, where these systems are efficient and mature, and using electrical heating for the final heating

52

to reduction temperature. This approach could benefit from many synergies with established technologies such as PV, as well as emerging technologies such as the Gen3 CSP [104] and electrically-charged TES [105]. Of course, such a system merits a robust physics-based technoeconomic analysis to evaluate their feasibility.

The isothermal cycle, which is often dismissed as less promising compared to the temperature-swing mode [26, 33, 32], may well be worth further investigating. However, future development should address the low feedstock conversion, with the most obvious route being to operate at higher temperatures. If high conversions can be achieved, the isothermal process has a lot of benefits over a temperature swing cycle, including the potential for rapid cycle times that can lead to greater power density, and a more promising outlook for scale-up.

Furthermore, perhaps an overall rethink of the research direction is required. For example the original cycles based on stoichiometric oxides, ZnO or Fe_3O_4, could be revisited, as the greater oxygen storage of these oxides offers a better outlook for higher efficiency and power density.

There are other reactor and process design concepts in the literature, which we have not addressed in detail here. One reoccurring theme is reactor systems which aim to address the issues of fixed bed reactors, via the application of moving redox particles [86, 106, 44], moving monoliths [23, 24, 87] or even moving reactors [88]. The main idea being that such systems can operate in a more continuous mode and incorporate heat recovery and countercurrent operation, which will improve the theoretical limits. These moving oxides systems do indeed have promise for improving the performance of this technology, but their complexity posses a daunting challenge.

Acknowledgements

References

[1] A. Steinfeld, Solar thermochemical production of hydrogen - A review, Solar Energy 78 (5) (2005) 603–615. `doi:10.1016/j.solener.2003.12.012`.

[2] Y. Mao, Y. Gao, W. Dong, H. Wu, Z. Song, X. Zhao, J. Sun, W. Wang, Hydrogen production via a two-step water splitting thermochemical cycle based on metal oxide–a review, Applied energy 267 (2020) 114860.

[3] V. K. Budama, J. P. R. Duarte, M. Roeb, C. Sattler, Potential of solar thermochemical water-splitting cycles: A review, Solar Energy 249 (2023) 353–366.

[4] K. J. Warren, A. W. Weimer, Solar thermochemical fuels: Present status and future prospects, Solar Compass 1 (2022) 100010. `doi:10.1016/j.solcom.2022.100010`.

[5] Y. Guo, J. Chen, H. Song, K. Zheng, J. Wang, H. Wang, H. Kong, A review of solar thermochemical cycles for fuel production, Applied Energy 357 (2024) 122499.

[6] G. Levêque, R. Bader, W. Lipiński, S. Haussener, High-flux optical systems for solar thermochemistry, Solar Energy 156 (2017) 133–148.

[7] M. Romero, A. Steinfeld, Concentrating solar thermal power and thermochemical fuels, Energy and Environmental Science 5 (11) (2012) 9234–9245. `doi:10.1039/c2ee21275g`.

[8] E. A. Fletcher, R. L. Moen, Hydrogen- and Oxygen from Water, Science 197 (4308) (1977) 1050–1056. `doi:10.1126/science.197.4308.1050`.

[9] J. E. Funk, R. M. Reinstrom, Energy requirements in production of hydrogen from water, Industrial & Engineering Chemistry Process Design and Development 5 (3) (1966) 336–342.

[10] R. Schäppi, D. Rutz, F. Dähler, A. Muroyama, P. Haueter, J. Lilliestam, A. Patt, P. Furler, A. Steinfeld, Drop-in Fuels from Sunlight and Air, Nature 601 (7891) (2021) 1–6. `doi:10.1038/s41586-021-04174-y`.

[11] V. Thanda, T. Fend, D. Laaber, A. Lidor, H. von Storch, J. Säck, J. Hertel, J. Lampe, S. Menz, G. Piesche, S. Berger, S. Lorentzou, M. Syrigou, T. Denk, A. Gonzales-Pardo, A. Vidal, M. Roeb, C. Sattler, Experimental investigation of the applicability of a 250 kW ceria receiver/reactor for solar thermochemical hydrogen generation, Renewable Energy 198 (August) (2022) 389–398. `doi:10.1016/j.renene.2022.08.010`.

[12] S. Zoller, E. Koepf, D. Nizamian, M. Stephan, A. Patané, P. Haueter, M. Romero, J. Gonzalez-Aguilar, D. Lieftink, E. de Wit, S. Brendelberger, A. Sizmann, A. Steinfeld, A solar tower fuel plant for the thermochemical production of kerosene from H_2O and CO_2, Joule 6 (2022) 1–11. `doi:10.1016/j.joule.2022.06.012`.

[13] C. Agrafiotis, M. Roeb, C. Sattler, 4.18 Solar Fuels, in: Comprehensive Energy Systems, Elsevier, 2018, pp. 733–761. `doi:10.1016/B978-0-12-809597-3.00429-6`.

[14] B. Bulfin, M. Miranda, A. Steinfeld, Performance Indicators for Benchmarking Solar Thermochemical Fuel Processes and Reactors, Frontiers in Energy Research 9 (July) (2021) 1–12. `doi:10.3389/fenrg.2021.677980`.

[15] L. Geissbühler, Thermocline Thermal Energy Storage: Advances and Applications to CSP, Compressed Air Energy Storage, and Solar Fuels, Phd dissertation, ETH Zürich (2017).

[16] O. Levenspiel, Chemical Reaction Engineering, John Wiley & Sons, 1999.

[17] E. Koepf, I. Alxneit, C. Wieckert, A. Meier, A review of high temperature solar driven reactor technology: 25 years of experience in research and development at the Paul Scherrer Institute, Applied Energy 188 (2017) 620–651. `doi:10.1016/j.apenergy.2016.11.088`.

[18] J. E. Miller, A. H. McDaniel, M. D. Allendorf, Considerations in the design of materials

for solar-driven fuel production using metal-oxide thermochemical cycles, Advanced Energy Materials 4 (2) (2014) 1300469.

[19] B. Bulfin, J. Vieten, C. Agrafiotis, M. Roeb, C. Sattler, Applications and limitations of two step metal oxide thermochemical redox cycles; a review, Journal of Materials Chemistry A 5 (36) (2017) 18951–18966. `doi:10.1039/C7TA05025A`.

[20] E. Koepf, W. Villasmil, A. Meier, Pilot-scale solar reactor operation and characterization for fuel production via the Zn/ZnO thermochemical cycle, Applied Energy 165 (2016) 1004–1023. `doi:10.1016/j.apenergy.2015.12.106`.

[21] N. Gokon, S. Takahashi, H. Yamamoto, T. Kodama, Thermochemical two-step water-splitting reactor with internally circulating fluidized bed for thermal reduction of ferrite particles, International Journal of Hydrogen Energy 33 (9) (2008) 2189–2199.

[22] W. C. Chueh, C. Falter, M. Abbott, D. Scipio, P. Furler, S. M. Haile, A. Steinfeld, High-flux solar-driven thermochemical dissociation of CO_2 and H_2O using ceria redox reactions, Science 330 (6012) (2010) 1797–1801. `doi:10.1123/science.1197834`.

[23] R. B. Diver, J. E. Miller, N. P. Siegel, T. A. Moss, Testing of a CR5 Solar Thermochemical Heat Engine Prototype, in: ASME 2010 4th International Conference on Energy Sustainability, Volume 2, ASMEDC, 2010, pp. 97–104. `doi:10.1115/ES2010-90093`.

[24] J. Miller, M. Allendorf, A. Ambrosini, E. Coker, R. Diver, Jr, I. Ermanoski, L. Evans, R. Hogan, Jr, A. McDaniel, Development and assessment of solar-thermal-activated fuel production. Phase 1, summary., Tech. Rep. SAND2012-5658, 1055617, Sandia National Laboratories (SNL), Albuquerque, NM, and Livermore, CA (United States) (Jul. 2012). `doi:10.2172/1055617`.

[25] W. Villasmil, A. Meier, A. Steinfeld, Dynamic modeling of a solar reactor for zinc oxide thermal dissociation and experimental validation using IR thermography, Journal of solar energy engineering 136 (1) (2014) 010901.

[26] B. J. Hathaway, R. Bala Chandran, A. C. Gladen, T. R. Chase, J. H. Davidson, Demonstration of a Solar Reactor for Carbon Dioxide Splitting via the Isothermal Ce-

ria Redox Cycle and Practical Implications, Energy & Fuels 30 (8) (2016) 6654–6661. `doi:10.1021/acs.energyfuels.6b01265`.

[27] D. Marxer, P. Furler, M. Takacs, A. Steinfeld, Solar thermochemical splitting of CO_2 into separate streams of CO and O_2 with high selectivity, stability, conversion, and efficiency, Energy Environ. Sci. 10 (5) (2017) 1142–1149. `doi:10.1039/C6EE03776C`.

[28] A. Haeussler, S. Abanades, A. Julbe, J. Jouannaux, B. Cartoixa, Solar thermochemical fuel production from H2O and CO2 splitting via two-step redox cycling of reticulated porous ceria structures integrated in a monolithic cavity-type reactor, Energy 201 (2020) 117649.

[29] I. Holmes-Gentle, S. Tembhurne, C. Suter, S. Haussener, Kilowatt-scale solar hydrogen production system using a concentrated integrated photoelectrochemical device, Nature Energy (2023) 1–11.

[30] R. J. Panlener, R. N. Blumenthal, J. E. Garnier, A thermodynamic study of nonstoichiometric cerium dioxide, Journal of Physics and Chemistry of Solids 36 (11) (1975) 1213–1222.

[31] N. R. Rhodes, M. M. Bobek, K. M. Allen, D. W. Hahn, Investigation of long term reactive stability of ceria for use in solar thermochemical cycles, Energy 89 (2015) 924–931.

[32] B. Bulfin, F. Call, M. Lange, O. Lübben, C. Sattler, R. Pitz-Paal, I. V. Shvets, Thermodynamics of CeO_2 Thermochemical Fuel Production, Energy & Fuels 29 (2) (2015) 1001–1009. `doi:10.1021/ef5019912`.

[33] I. Ermanoski, J. Miller, M. Allendorf, Efficiency maximization in solar-thermochemical fuel production: challenging the concept of isothermal water splitting, Physical Chemistry Chemical Physics 16 (18) (2014) 8418–8427.

[34] D. Marxer, P. Furler, J. Scheffe, H. Geerlings, C. Falter, V. Batteiger, A. Sizmann, A. Steinfeld, Demonstration of the entire production chain to renewable kerosene via

solar thermochemical splitting of H_2O and CO_2, Energy and Fuels 29 (5) (2015) 3241–3250. `doi:10.1021/acs.energyfuels.5b00351`.

[35] S. Abanades, A. Haeussler, Two-step thermochemical cycles using fibrous ceria pellets for H_2 production and CO_2 reduction in packed-bed solar reactors, Sustainable Materials and Technologies 29 (2021) e00328.

[36] R. Schäppi, D. Rutz, P. Basler, A. Muroyama, P. Haueter, P. Furler, A. Steinfeld, Solar thermochemical splitting of CO_2 in a modular solar dish-reactor system, in: Proceedings of the ISES Solar World Congress 2019 and IEA SHC International Conference on Solar Heating and Cooling for Buildings and Industry 2019, International Solar Energy Society, 2019, pp. 1405–1408. `doi:10.18086/swc.2019.24.08`.

[37] A. Lidor, T. Fend, M. Roeb, C. Sattler, High performance solar receiver–reactor for hydrogen generation, Renewable Energy 179 (2021) 1217–1232. `doi:10.1016/j.renene.2021.07.089`.

[38] E. Koepf, S. Zoller, S. Luque, M. Thelen, S. Brendelberger, J. González-Aguilar, M. Romero, A. Steinfeld, Liquid fuels from concentrated sunlight: An overview on development and integration of a 50 kW solar thermochemical reactor and high concentration solar field for the SUN-to-LIQUID project, in: AIP conference proceedings, Vol. 2126, AIP Publishing, 2019.

[39] J. Gallagher, Tower of achievement, Nature Energy 7 (8) (2022) 680–680.

[40] M. Hoes, S. Ackermann, D. Theiler, P. Furler, A. Steinfeld, Additive-Manufactured Ordered Porous Structures Made of Ceria for Concentrating Solar Applications, Energy Technology 7 (9) (2019). `doi:10.1002/ente.201900484`.

[41] B. A. Ben-Arfa, S. Abanades, I. M. M. Salvado, J. M. Ferreira, R. C. Pullar, Robocasting of 3d printed and sintered ceria scaffold structures with hierarchical porosity for solar thermochemical fuel production from the splitting of co 2, Nanoscale 14 (13) (2022) 4994–5001.

[42] S. Sas Brunser, F. L. Bargardi, R. Libanori, N. Kaufmann, H. Braun, A. Steinfeld, A. R. Studart, Solar-driven redox splitting of co2 using 3d-printed hierarchically channeled ceria structures, Advanced Materials Interfaces (2023) 2300452.

[43] A. Eltayeb, V. Graß, K. Lee, M. Pein, C. Agrafiotis, M. Schmücker, M. Roeb, C. Sattler, Characterisation and thermochemical stability analysis of 3d printed porous ceria structures fabricated via composite extrusion modelling, Materials & Design 236 (2023) 112514.

[44] S. Li, V. M. Wheeler, P. B. Kreider, R. Bader, W. Lipiński, Thermodynamic Analyses of Fuel Production via Solar-Driven Non-stoichiometric Metal Oxide Redox Cycling. Part 2. Impact of Solid–Gas Flow Configurations and Active Material Composition on System-Level Efficiency, Energy & Fuels 32 (10) (2018) 10848–10863. `doi:10.1021/acs.energyfuels.8b02082`.

[45] M. L. T. Triviño, N. C. Arriola Jr, Y. S. Kang, J. G. Seo, Transforming co2 to valuable feedstocks: Emerging catalytic and technological advances for the reverse water gas shift reaction, Chemical Engineering Journal (2024) 150369.

[46] C. Falter, A. Valente, A. Habersetzer, D. Iribarren, J. Dufour, An integrated techno-economic, environmental and social assessment of the solar thermochemical fuel pathway, Sustainable Energy and Fuels 4 (8) (2020) 3992–4002. `doi:10.1039/d0se00179a`.

[47] Z. Ma, P. Davenport, G. Saur, System and technoeconomic analysis of solar thermochemical hydrogen production, Renewable Energy 190 (2022) 294–308, publisher: Elsevier Ltd. `doi:10.1016/j.renene.2022.03.108`.

[48] C. Moretti, V. Patil, C. Falter, L. Geissbühler, A. Patt, A. Steinfeld, Technical, economic and environmental analysis of solar thermochemical production of drop-in fuels, Science of The Total Environment (2023) 166005.

[49] A. H. Alami, A. G. Olabi, A. Mdallal, A. Rezk, A. Radwan, S. M. A. Rahman, S. K. Shah, M. A. Abdelkareem, Concentrating solar power (CSP) technologies: Status and analysis, International Journal of Thermofluids 18 (2023) 100340.

[50] J. Lilliestam, L. Ollier, M. Labordena, S. Pfenninger, R. Thonig, The near-to mid-term outlook for concentrating solar power: mostly cloudy, chance of sun, Energy Sources, Part B: Economics, Planning, and Policy 16 (1) (2021) 23–41.

[51] S. Li, V. M. Wheeler, A. Kumar, M. B. Venkataraman, C. L. Muhich, Y. Hao, W. Lipiński, Thermodynamic Guiding Principles for Designing Nonstoichiometric Redox Materials for Solar Thermochemical Fuel Production: Ceria, Perovskites, and Beyond, Energy Technology 2000925 (19) (2021) 1–18. `doi:10.1002/ente.202000925`.

[52] M. Hoes, C. L. Muhich, R. Jacot, G. R. Patzke, A. Steinfeld, Thermodynamics of paired charge-compensating doped ceria with superior redox performance for solar thermochemical splitting of H_2O and CO_2, Journal of Materials Chemistry A 5 (36) (2017) 19476–19484. `doi:10.1039/C7TA05824A`.

[53] J. R. Scheffe, A. Steinfeld, Thermodynamic analysis of cerium-based oxides for solar thermochemical fuel production, Energy & Fuels 26 (3) (2012) 1928–1936. `doi:10.1021/ef201875v`.

[54] C. L. Muhich, S. Blaser, M. C. Hoes, A. Steinfeld, Comparing the solar-to-fuel energy conversion efficiency of ceria and perovskite based thermochemical redox cycles for splitting H2O and CO2, International Journal of Hydrogen Energy 43 (41) (2018) 18814–18831. `doi:10.1016/j.ijhydene.2018.08.137`.

[55] S. Li, V. M. Wheeler, P. B. Kreider, W. Lipiński, Thermodynamic Analyses of Fuel Production via Solar-Driven Non-stoichiometric Metal Oxide Redox Cycling. Part 1. Revisiting Flow and Equilibrium Assumptions, Energy & Fuels 32 (10) (2018) 10838–10847. `doi:10.1021/acs.energyfuels.8b02081`.

[56] M. Lin, S. Haussener, Solar fuel processing efficiency for ceria redox cycling using alternative oxygen partial pressure reduction methods, Energy 88 (2015) 667–679. `doi:10.1016/j.energy.2015.06.006`.

[57] C. P. Falter, R. Pitz-Paal, Modeling counter-flow particle heat exchangers for two-step

solar thermochemical syngas production, Applied Thermal Engineering 132 (2018) 613–623. `doi:10.1016/j.applthermaleng.2017.12.087`.

[58] B. Bulfin, L. Hoffmann, L. de Oliveira, N. Knoblauch, F. Call, M. Roeb, C. Sattler, M. Schmücker, Statistical thermodynamics of non-stoichiometric ceria and ceria zirconia solid solutions, Physical Chemistry Chemical Physics 18 (33) (2016) 23147–23154. `doi:10.1039/C6CP03158G`.

[59] S. Brendelberger, M. Roeb, M. Lange, C. Sattler, Counter flow sweep gas demand for the ceria redox cycle, Solar Energy 122 (2015) 1011–1022. `doi:10.1016/j.solener.2015.10.036`.

[60] X. Qian, J. He, E. Mastronardo, B. Baldassarri, C. Wolverton, S. M. Haile, Favorable redox thermodynamics of $SrTi_{0.5}Mn_{0.5}O_{3-\delta}$ in solar thermochemical water splitting, Chemistry of Materials 32 (21) (2020) 9335–9346.

[61] S. Zhai, J. Rojas, N. Ahlborg, K. Lim, M. F. Toney, H. Jin, W. C. Chueh, A. Majumdar, The use of poly-cation oxides to lower the temperature of two-step thermochemical water splitting, Energy & Environmental Science 11 (8) (2018) 2172–2178.

[62] R. J. Carrillo, J. R. Scheffe, Advances and trends in redox materials for solar thermochemical fuel production, Solar Energy 156 (2017) 3–20. `doi:10.1016/j.solener.2017.05.032`.

[63] B. Bulfin, M. Lange, L. de Oliveira, M. Roeb, C. Sattler, Solar thermochemical hydrogen production using ceria zirconia solid solutions: Efficiency analysis, International Journal of Hydrogen Energy 41 (42) (2016) 19320–19328. `doi:10.1016/j.ijhydene.2016.05.211`.

[64] J. Vieten, B. Bulfin, P. Huck, M. Horton, D. Guban, L. Zhu, Y. Lu, K. A. Persson, M. Roeb, C. Sattler, Materials design of perovskite solid solutions for thermochemical applications, Energy & Environmental Science 12 (4) (2019) 1369–1384.

[65] Y. Hao, C.-K. Yang, S. M. Haile, Ceria–zirconia solid solutions ($Ce_{1-x}Zr_xO_{2-\delta}$, $x \leq$

0.2) for solar thermochemical water splitting: A thermodynamic study, Chemistry of Materials 26 (20) (2014) 6073–6082. `doi:10.1021/cm503131p`.

[66] A. Haeussler, S. Abanades, J. Jouannaux, A. Julbe, Non-stoichiometric redox active perovskite materials for solar thermochemical fuel production: A review, Catalysts 8 (12) (2018) 611.

[67] T. Cooper, J. R. Scheffe, M. E. Galvez, R. Jacot, G. Patzke, A. Steinfeld, Lanthanum manganite perovskites with CaSr A-site and Al B-site doping as effective oxygen exchange materials for solar thermochemical fuel production, Energy Technology 3 (11) (2015) 1130–1142.

[68] S. Zhai, J. Rojas, N. Ahlborg, K. Lim, C. H. M. Cheng, C. Xie, M. F. Toney, I.-H. Jung, W. C. Chueh, A. Majumdar, High-capacity thermochemical CO_2 dissociation using iron-poor ferrites, Energy & Environmental Science 13 (2) (2020) 592–600.

[69] G. Lenarduzzi, T. A. Cooper, The role of entropy in the success of nonstoichiometric oxides for two-step thermochemical water and co2 splitting, Applied Physics Letters 119 (26) (2021).

[70] J. M. Naik, C. Ritter, B. Bulfin, A. Steinfeld, R. Erni, G. R. Patzke, Reversible phase transformations in novel Ce-substituted perovskite oxide composites for solar thermochemical redox splitting of CO_2, Advanced Energy Materials 11 (16) (2021) 2003532.

[71] S. Brendelberger, J. Vieten, M. J. Vidyasagar, M. Roeb, C. Sattler, Demonstration of thermochemical oxygen pumping for atmosphere control in reduction reactions, Solar Energy 170 (2018) 273–279.

[72] S. A. Wilson, E. B. Stechel, I. Ermanoski, C. L. Muhich, Substituted ALPO-5 zeolites as promising O_2 sorption pump materials: A density functional theory study, The Journal of Physical Chemistry C 125 (2) (2021) 1269–1281.

[73] I. Ermanoski, Cascading pressure thermal reduction for efficient solar fuel production, International journal of hydrogen energy 39 (25) (2014) 13114–13117.

[74] C. L. Muhich, B. W. Evanko, K. C. Weston, P. Lichty, X. Liang, J. Martinek, C. B. Musgrave, A. W. Weimer, Efficient generation of H2 by splitting water with an isothermal redox cycle, Science 341 (6145) (2013) 540–542.

[75] K. J. Warren, J. T. Tran, A. W. Weimer, A thermochemical study of iron aluminate-based materials: A preferred class for isothermal water splitting, Energy and Environmental Science 15 (2022) 806–821. `doi:10.1039/d1ee02679h`.

[76] K. Lee, D. C. McCord, R. J. Carrillo, B. Guyll, J. R. Scheffe, Improved performance and efficiency of lanthanum–strontium–manganese perovskites undergoing isothermal redox cycling under controlled p H2O/p H2, Energy & Fuels 34 (12) (2020) 16918–16926.

[77] R. J. Carrillo, J. R. Scheffe, Beyond ceria: theoretical investigation of isothermal and near-isothermal redox cycling of perovskites for solar thermochemical fuel production, Energy & Fuels 33 (12) (2019) 12871–12884.

[78] J. T. Tran, K. J. Warren, D. Mejic, R. L. Anderson, L. Jones, D. S. Hauschulz, C. Wilson, A. W. Weimer, Pressure-enhanced performance of metal oxides for thermochemical water and carbon dioxide splitting, Joule 7 (8) (2023) 1759–1768.

[79] R. Bader, L. J. Venstrom, J. H. Davidson, W. Lipiński, Thermodynamic Analysis of Isothermal Redox Cycling of Ceria for Solar Fuel Production, Energy & Fuels 27 (9) (2013) 5533–5544. `doi:10.1021/ef400132d`.

[80] B. D. Ehrhart, C. L. Muhich, I. Al-Shankiti, A. W. Weimer, System efficiency for two-step metal oxide solar thermochemical hydrogen production – Part 1: Thermodynamic model and impact of oxidation kinetics, International Journal of Hydrogen Energy 41 (44) (2016) 19881–19893. `doi:10.1016/j.ijhydene.2016.07.109`.

[81] B. D. Ehrhart, C. L. Muhich, I. Al-Shankiti, A. W. Weimer, System efficiency for two-step metal oxide solar thermochemical hydrogen production – Part 2: Impact of gas heat recuperation and separation temperatures, International Journal of Hydrogen Energy 41 (44) (2016) 19894–19903. `doi:10.1016/j.ijhydene.2016.07.110`.

[82] S. Abanades, A. Legal, A. Cordier, G. Peraudeau, G. Flamant, A. Julbe, Investigation of reactive cerium-based oxides for H2 production by thermochemical two-step water-splitting, Journal of Materials Science 45 (15) (2010) 4163–4173. `doi:10.1007/s10853-010-4506-4`.

[83] P. Furler, J. Scheffe, D. Marxer, M. Gorbar, A. Bonk, U. Vogt, A. Steinfeld, Thermochemical CO_2 splitting via redox cycling of ceria reticulated foam structures with dual-scale porosities, Physical Chemistry Chemical Physics 16 (22) (2014) 10503–10511. `doi:10.1039/c4cp01172d`.

[84] A. Lidor, Y. Aschwanden, J. Häseli, P. Reckinger, P. Haueter, A. Steinfeld, High-temperature heat recovery from a solar reactor for the thermochemical redox splitting of H_2O and CO_2, Applied Energy 329 (November 2022) (2023) 120211. `doi:10.1016/j.apenergy.2022.120211`.

[85] J. Lapp, W. Lipiński, Transient Three-Dimensional Heat Transfer Model of a Solar Thermochemical Reactor for H_2O and CO_2 Splitting Via Nonstoichiometric Ceria Redox Cycling, Journal of Solar Energy Engineering 136 (3) (2014) 031006. `doi:10.1115/1.4026465`.

[86] J. Felinks, S. Brendelberger, M. Roeb, C. Sattler, R. Pitz-Paal, Heat recovery concept for thermochemical processes using a solid heat transfer medium, Applied Thermal Engineering 73 (1) (2014) 1006–1013. `doi:10.1016/j.applthermaleng.2014.08.036`.

[87] S. Siegrist, H. von Storch, M. Roeb, C. Sattler, Moving Brick Receiver–Reactor: A Solar Thermochemical Reactor and Process Design With a Solid–Solid Heat Exchanger and On-Demand Production of Hydrogen and/or Carbon Monoxide, Journal of Solar Energy Engineering 141 (2) (2019) 021009. `doi:10.1115/1.4042069`.

[88] A. S. Patankar, X.-Y. Wu, W. Choi, H. L. Tuller, A. F. Ghoniem, A Reactor Train System for Efficient Solar Thermochemical Fuel Production, Journal of Solar Energy Engineering 144 (6) (2022) 1–12. `doi:10.1115/1.4055298`.

[89] A. Lidor, L. Zimmermann, Experimental demonstration of high-temperature heat recovery in a solar reactor, Solar Energy 262 (2023) 111915. `doi:10.1016/j.solener.2023.111915`.

[90] S. Brendelberger, P. Holzemer-Zerhusen, H. von Storch, C. Sattler, Performance Assessment of a Heat Recovery System for Monolithic Receiver-Reactors, Journal of Solar Energy Engineering 141 (2) (2019) 021008. `doi:10.1115/1.4042241`.

[91] L. Geissbühler, A. Mathur, A. Mularczyk, A. Haselbacher, An assessment of thermocline-control methods for packed-bed thermal-energy storage in CSP plants, Part 1: Method descriptions, Solar Energy 178 (2019) 341–350. `doi:10.1016/j.solener.2018.12.015`.

[92] P. Roos, A. Haselbacher, Thermocline control through multi-tank thermal-energy storage systems, Applied Energy 281 (2021) 115971. `doi:10.1016/j.apenergy.2020.115971`.

[93] L. André, S. Abanades, G. Flamant, Screening of Thermochemical Systems Based on Solid-Gas Reversible Reactions for High Temperature Solar Thermal Energy Storage, Renewable and Sustainable Energy Reviews 64 (2016) 703–715. `doi:10.1016/j.rser.2016.06.043`.

[94] S. Lorentzou, A. Zygogianni, C. Pagkoura, G. Karagiannakis, A. G. Konstandopoulos, J. P. Saeck, S. Breuer, M. Lange, J. Lapp, T. Fend, M. Roeb, A. J. Gonzalez, A. V. Delgado, J. P. Brouwer, R. C. Makkus, S. J. Kiartzis, HYDROSOL-PLANT: Structured redox reactors for H_2 production from solar thermochemical H_2O splitting, in: SolarPACES 2017: International Conference on Concentrating Solar Power and Chemical Energy Systems, Santiago, Chile, 2018, p. 130010. `doi:10.1063/1.5067144`.

[95] J. Grobbel, M. F. Sollich, D. M. Quinto, A. Lidor, C. Sattler, Operation optimization of an array of receiver-reactors for solar fuel production, AIP Conference Proceedings 2445 (1) (2022) 130004. `doi:10.1063/5.0085738`.

[96] World demand by product groups, 2018-2019 (2021).

URL `https://www.iea.org/data-and-statistics/charts/world-demand-by-product-groups-2018-2019`

[97] Product Supplied for Kerosene-Type Jet Fuel (2023).

URL `https://www.eia.gov/dnav/pet/pet_cons_psup_a_EPJK_VPP_mbbl_a.htm`

[98] Sustainability report, Tech. rep., Lufthansa Group (2019).

URL `https://www.lufthansagroup.com/en/responsibility/reports.html`

[99] S. Wietlisbach, A. Gao, Rare Earth Minerals and Products, Tech. rep., S&P Global (Jun. 2023).

[100] L. Li, B. Wang, J. Pye, W. Lipiński, Temperature-based optical design, optimization and economics of solar polar-field central receiver systems with an optional compound parabolic concentrator, Solar energy 206 (2020) 1018–1032.

[101] B. Bulfin, M. Zuber, O. Gräub, A. Steinfeld, Intensification of the reverse water–gas shift process using a countercurrent chemical looping regenerative reactor, Chemical Engineering Journal 461 (4 2023). `doi:10.1016/j.cej.2023.141896`.

[102] I. S. Metcalfe, B. Ray, C. Dejoie, W. Hu, C. de Leeuwe, C. Dueso, F. R. García-García, C.-M. Mak, E. I. Papaioannou, C. R. Thompson, et al., Overcoming chemical equilibrium limitations using a thermodynamically reversible chemical reactor, Nature Chemistry 11 (7) (2019) 638–643.

[103] H. von Storch, M. Roeb, H. Stadler, C. Sattler, A. Bardow, B. Hoffschmidt, On the assessment of renewable industrial processes: Case study for solar co-production of methanol and power, Applied Energy 183 (2016) 121–132. `doi:10.1016/j.apenergy.2016.08.141`.

[104] M. Mehos, C. Turchi, J. Vidal, M. Wagner, Z. Ma, C. Ho, W. Kolb, C. Andraka, A. Kruizenga, Concentrating solar power gen3 demonstration roadmap, Tech. rep., National Renewable Energy Lab.(NREL), Golden, CO (United States) (2017).

[105] Z. Ma, J. Gifford, X. Wang, J. Martinek, Electric-thermal energy storage using solid particles as storage media, Joule 7 (5) (2023) 843–848.

[106] C. P. Falter, R. Pitz-Paal, A generic solar-thermochemical reactor model with internal heat diffusion for counter-flow solid heat exchange, Solar Energy 144 (2017) 569–579. `doi:10.1016/j.solener.2017.01.063`.